THESIS

DEVELOPMENT OF A MODEL FOR BAFFLE ENERGY DISSIPATION IN LIQUID FUELED ROCKET ENGINES

Submitted by

Nathan A. Miller

Department of Mechanical Engineering

In partial fulfillment of the requirements

For the Degree of Master of Science

Colorado State University

Fort Collins, Colorado

Fall 2010

COLORADO STATE UNIVERSITY

August 26, 2010

WE HEREBY RECOMMEND THAT THE THESIS PREPARED UNDER OUR SUPERVISION BY NATHAN MILLER ENTITLED DEVELOPMENT OF A MODEL FOR BAFFLE ENERGY DISSIPATION IN LIQUID FUELED ROCKET ENGINES BE ACCEPTED AS FULFULLING IN PART REQUIREMENTS FOR THE DEGREE OF MASTER OF SCIENCE.

Committee on Graduate Work

_____
Jeanne Duflot

_____
John D. Williams

_____
Advisor: Allan T. Kirkpatrick

_____
Department Head: Susan P. James

ABSTRACT OF THESIS

DEVELOPMENT OF A MODEL FOR BAFFLE ENERGY DISSIPATION
IN LIQUID FUELED ROCKET ENGINES

In this thesis the energy dissipation from a combined hub and blade baffle structure in a combustion chamber of a liquid-fueled rocket engine is modeled and computed. An analytical model of the flow stabilization due to the effect of combined radial and hub blades was developed. The rate of energy dissipation of the baffle blades was computed using a corner-flow model that included unsteady flow separation and turbulence effects. For the inviscid portion of the flow field, a solution methodology was formulated using an eigenfunction expansion and a velocity potential matching technique. Parameters such as local velocity, elemental path length, effective viscosity, and local energy dissipation rate were computed as a function of the local angle α for a representative baffle blade, and compared to results predicted by the Baer-Mitchell blade dissipation model. The sensitivity of the model to the overall engine acoustic oscillation mode, blade length, and thickness was also computed and compared to previous results.

Additional studies were performed to determine the sensitivity to input parameters such as the dimensionless turbulence coefficient, the location of the potential difference in the generation of the dividing streamline, the number of baffle blades and the size of the central hub. Stability computations of a test engine indicated that when the baffle length is increased, the

baffles provide increased stabilization effects. The model predicts greatest dissipation for radial modes with a hub radius at approximately half the chamber's radius.

Nathan A. Miller
Department of Mechanical Engineering
Colorado State University
Fort Collins, CO 80523
Fall 2010

Table of Contents

List of Figures

List of Symbols

a	Constant defined by potential at specific location
c_1	Turbulence coefficient (Corner-flow)
c_{turb}	Turbulence coefficient (Baer-Mitchell)
E_{diss}	Energy dissipation rate
k	Constant defined by potential at specific location
r	Radial coordinate
r_h	Hub Radius
r_o	Chamber Radius
s	Streamwise coordinate
t	Baffle blade thickness
u	Oscillating velocity over baffle blade
U	Mean flow velocity
v_{diss}	Total dissipation over baffle structure
y	Coordinate normal to streamline
z	Axial coordinate
z_b	Baffle length
z_{match}	Position at which potential difference is taken

Greek Symbols

α	Angular position on streamline
δ	Penetration depth
ε	Pressure oscillation
θ	Azimuthal baffle angle
λ	Damping Rate
ρ	Density
μ	Dynamic viscosity
ν_{eff}	Effective kinematic viscosity
ζ	Local streamline radius
ω	Frequency
φ	Potential
Ψ	Streamfunction

1: Introduction

Liquid propellant rocket engines are susceptible to high-frequency combustion instability, a coupling between the acoustics of the combustion chamber and the combustion process. The stochastic pressure oscillations caused by the combustion process add energy to the system in such a way as to promote organization into an acoustic-type wave or mode. These acoustically coupled oscillations adversely impact engine performance through increased rates of heat transfer to the injector face and combustion chamber walls and by inducing excessive structural vibrations. In extreme cases, instability of this sort can result in engine failure.

The acoustic oscillations of interest have been low-order tangential and radial modes. To reduce the detrimental effects of the oscillatory instability, these vibrations can be dampened using injector face baffles. While many different arrangements of baffles are used to dampen oscillations, two common types of baffles include the hub and radial types. Hub baffles are used to reduce radial oscillations, while radial blade baffles have been used to reduce the tangential oscillations. Hub baffles also have some effect on tangential modes though it is minimal at best. Radial baffle blades have essentially no effect on the radial modes due to the symmetric nature of the pressure distribution on either side of the blade.

In addition to increased viscous dissipation, the baffle effects also include a decrease in the acoustic frequency of a rocket engine, as the baffles increase the oscillation path length. It is through a mechanism of viscous drag that the blades are believed to reduce the strength of the pressure oscillations and increase the overall stability of the combustion process. An unfortunate side effect of these baffle blades is a reduction in engine thrust, however; this negative effect is negligible when compared to the detrimental effects of uncontrolled, large amplitude chamber pressure oscillation. In this thesis the energy dissipation from a combined hub and blade baffle

structure in a combustion chamber, as shown in Figure 1, is modeled and computed. It should be noted that the radial baffle blades are not required to be spaced evenly as shown in the figure. There are benefits and detriments for both arrangements. Throughout this thesis, an even spacing among the radial baffles is assumed to coincide with previous published works. In addition, while it is possible to have multiple hub baffles to counter radial modes of larger order, such geometries are not modeled herein. The techniques used for a singular annular baffle however, could be applied to these more complex structures.

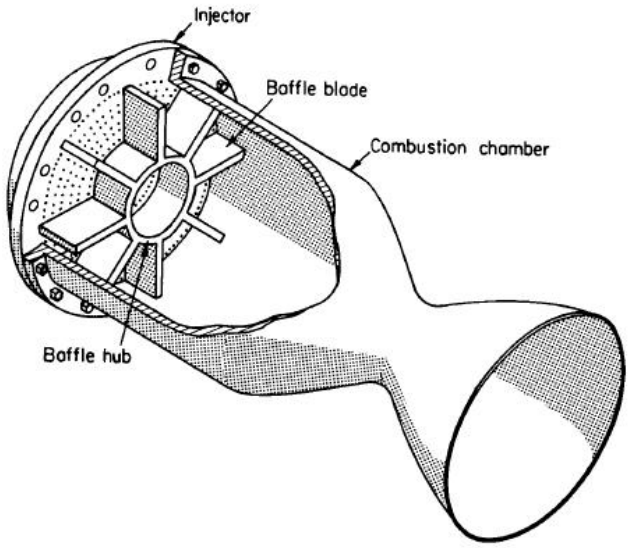

Figure 1. Baffle blade and hub in combustion chamber (from Harrje and Reardon[1])

2: Background

2.1: Vibration Geometry

Pressure oscillations in combustion chambers can be described by the solution of the forced Helmholtz equation (Equation 1).

$$\nabla^2 \cdot \phi + \omega^2 \cdot \phi = F(\phi) \qquad (1)$$

The Helmholtz equation can be solved through the separation of variables using an eigenfunction matching technique. This method assumes that the different axes are independent of each other. This assumption means that the oscillation must be linear resulting in an Equation 2.

$$\phi(r, \theta, z) = R(r) \cdot \Theta(\theta) \cdot Z(z) \qquad (2)$$

Appendix 1 shows the derivation of the two dimensional, no dependence on the axial position z, oscillatory case. It also demonstrates that the difference between a thin fluid sheet and a thin film oscillating is in the boundary conditions.

The pressure oscillations present in combustion chambers can be of three major shapes. Radial modes are oscillations in the radial direction, tangential modes have both a radial and angular dependance and longitudinal modes are oscillations in the axial direction. It is possible for combination modes to exist. An example of this is a 1T1R mode where a tangential mode is combined with a radial mode. In DISTCS, the engine stability code used for these calculations, the longitudinal mode is unconstrained and allowed to vary freely. The mode shapes can be

either standing or spinning modes. Standing modes only vary in amplitude as a function of time while spinning modes rotate around the longitudinal axis. Examples of standing modes are shown in Figure 2. A spinning 1T mode is shown in Figure 3.

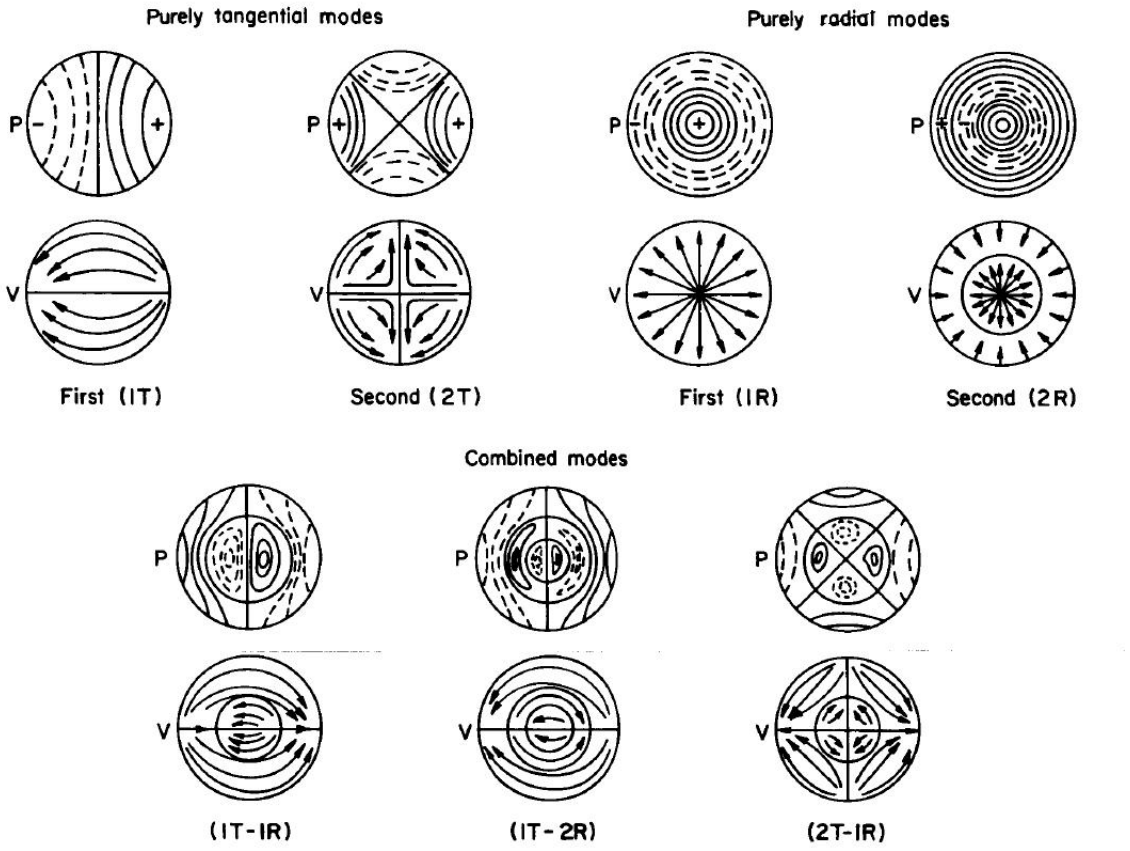

Figure 2: Example pressure and velocity oscillation profiles in an unbaffled chamber (from Harrje and Reardon[1])

Oscillations solved using eigenfunction techniques are denoted by their indices of vibration. In this thesis the mode number and shape are defined by (m,l,n). The radial indices are indicated by n, tangential indices are indicated by l, and longitudinal indices are indicated by n. The radial indices begin at 1 while the tangential and longitudinal indices begin at 0. This is due to the formulation of the Bessel functions. A 1T mode as shown above will have the indices

(1,1,0). A 1R mode will have the indices (0,2,0). A 1T1R mode would be indicated by the indices (1,2,0).

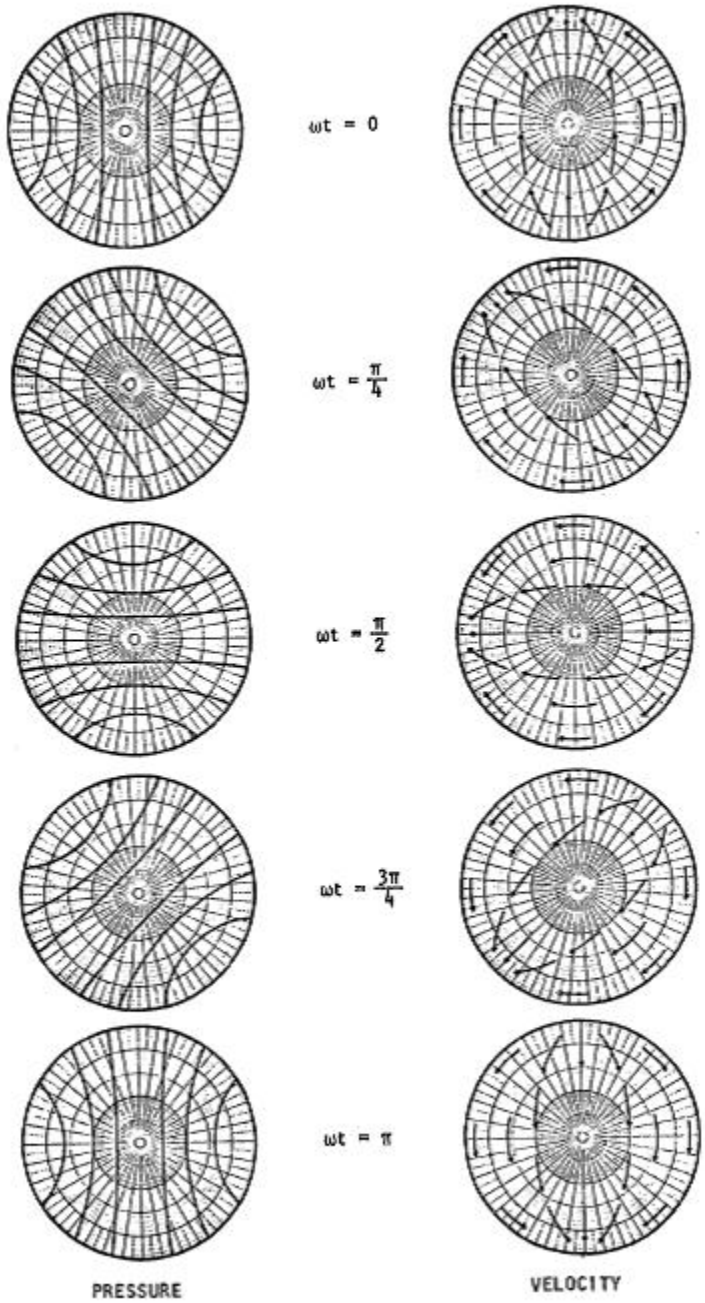

Figure 3: Pressure and velocity distributions for 1T spinning mode (from Harrje and Reardon[1])

Different arrangements of baffles will have different effects on different modes. Some baffle structures will actually fall into the nodes of the pressure potential. This is shown in Figure 4. Note that radial modes are totally unaffected by radial baffles of any configuration. These modes can only be reduced with hub baffles. In addition a baffle structure of four radial blades and no central hub is completely ineffective in any dissipation. It is for these reasons that baffle arrangements typically are combinations of radial and hub shaped baffles. The number of radial baffles are also typically prime numbers and greater than any of the tangential modes observed.

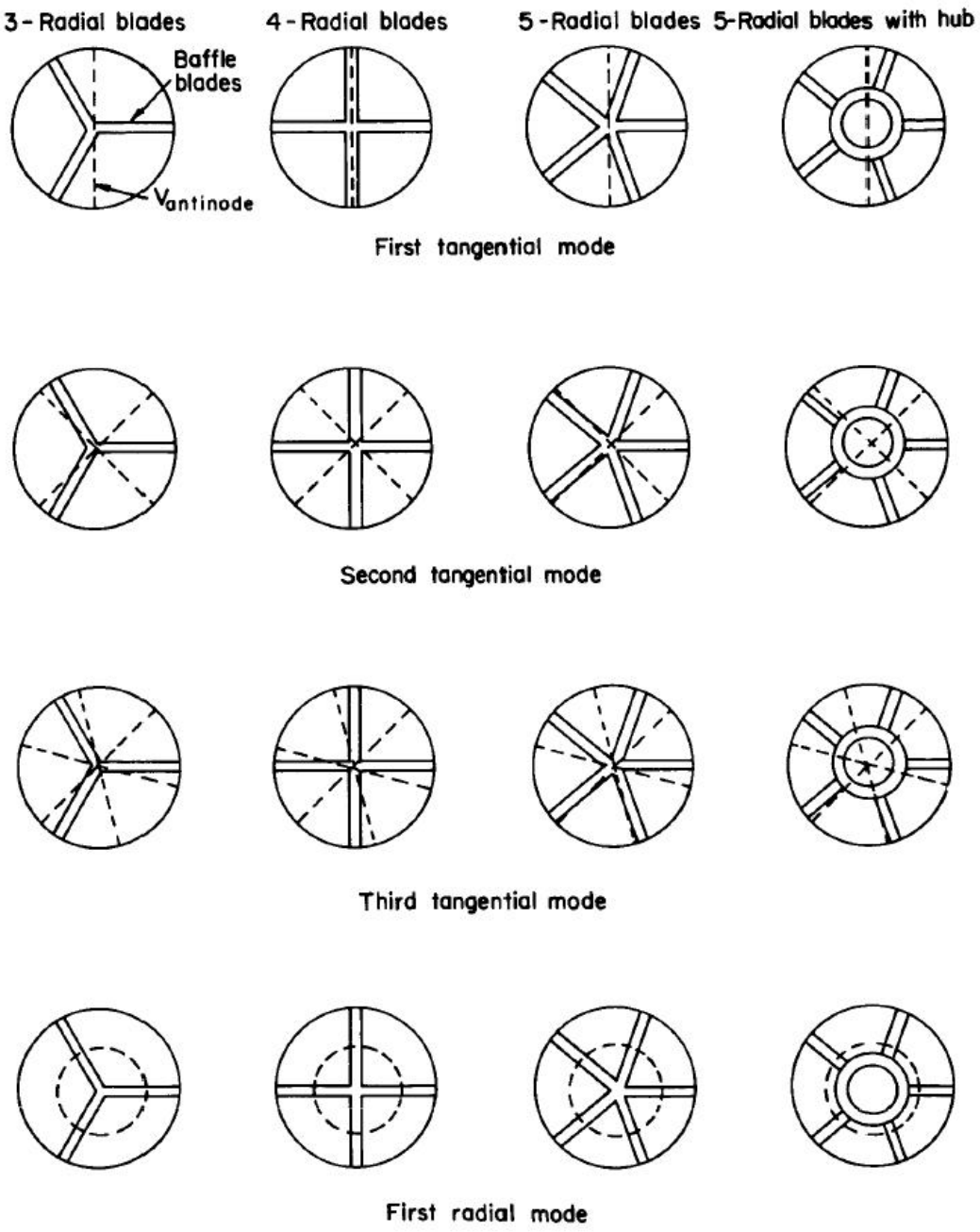

Figure 4: Anti-Node alignment with different baffle arrangements (from Harrje and Reardon[1])

2.2: Non-dimensional Scheme

Non-dimensionalizing the variables is very useful in the development of the potential equations. By removing the dimensional dependance the complexity of the potential equations is

reduced. Dimensional variables (indicated by a * superscript) such as time, frequency, and various lengths are non-dimensionalized by the chamber radius, r_c*, and the dimensional speed of sound at the stagnation condition a_0*. Examples of non-dimensional equations are given below. Equation 3a demonstrates the non-dimensionalization of the frequency of oscillation while Equation 3b is the non-dimensionalization of time and Equation 3c is the non-dimensionalization of distance. An expanded look at non-dimensionalization is included in Appendix 2.

$$\omega = 2 \cdot \pi \cdot f^* \cdot \frac{r_c^*}{a_0^*} \tag{3a}$$

$$t = t^* \cdot \frac{\bar{a}_0^*}{r_c^*} \tag{3b}$$

$$x = \frac{x^*}{r_c^*} \tag{3c}$$

2.3: Combustion Stability Review

A comprehensive overview of combustion instability research in liquid rocket engines is given in Harrje and Reardon[1], and a review of various analytical approaches used to model this problem is given in Mitchell[2]. The combustion stability analysis of Mitchell[2] utilized the non-dimensional governing equations in a velocity potential formulation, using the chamber radius, the speed of sound at the nozzle entrance, and the stagnation pressure to non-dimensionalize the length, velocity, and pressure scales. Using a perturbation technique and a linearization process, the equations were combined into a single linear, second order, non-homogenous, Helmholtz equation. The velocity potential was assumed to be harmonic and solved for in each compartment of interest subject to boundary conditions and a matching condition with adjacent compartments where necessary.

As the velocity potential is assumed to be harmonic, the frequency can be assumed to be a complex value with the real part describing the oscillatory frequency and the imaginary part

describing the decay. The frequency is then non-dimensionalized using the chamber radius and the speed of sound in the chamber. Due to the complex geometry of the overall combustion chamber a direct solution of the potential equations would be impossible with a simple separation of variables approach. Instead as described in Baer and Mitchell[3] as well as Milano[4] an eigenfunction matching technique between different chamber volumes is employed. For example, the eigenfunction solution to the potential distribution of a standing wave, in a chamber without baffles takes the form:

References to combustion stability in this thesis typically refer to calculations of the overall n and τ. The variable n is the interaction index or, to clarify, it is the gain parameter of the combustion pressure perturbation. The variable τ is the time lag between the combustion response and the pressure fluctuation. To describe it in a different way, it is the time delay between a pressure oscillation and when the combustion responds to it. Given these variables and angular frequency ω it is possible to calculate the value of a stability parameter N also called CRES. CRES is an overall measure of the combustion response of the engine and is the ratio of the non-dimensional oscillatory gas generation to oscillatory pressure shown in Equation 4.

$$N = \frac{\frac{Q'}{\bar{Q}}}{\frac{P'}{\bar{P}}} \qquad (4)$$

CRES is a complex variable with magnitude and phase, and is related to n and τ by the following equation.

$$|N| = \left| n \cdot \left(1 - e^{-i \cdot \omega \cdot \tau} \right) \right| \qquad (5)$$

In practice, typical n values range from 0.5 to 1 and typical τ values range from 0.3 to 3. The values of n and τ are often used as a method of classifying different injector/propellant

combinations. The stability is plotted on n-τ or |N|-ω coordinates shown in Figures 36-44 presented later in the thesis, with a minimum point along the curve indicating minimum stability.

The instabilities referred to in this paper are typically called high-frequency instabilities and are a result of the combustion process triggering the fundamental acoustic frequencies of the combustion chamber. These instabilities are some of the most critical in determining engine performance and the overall safety of the rocket. While lower frequency instabilities are typically associated with the overall structure and intermediate frequencies are relatively non-destructive, high frequencies are directly tied to the performance of the combustion chamber and can be particularly damaging.

$$\phi = e^{i\cdot\omega\cdot t}\cdot\sum_{m,l} A_{m,l}\cdot\left[\cos(m\cdot\theta)\cdot J_m(\lambda_{m,l}\cdot r)\cdot\cos(\frac{n\cdot\pi\cdot z}{L})\right] \quad (6)$$

For equation (6), φ is the velocity potential in the chamber, $\lambda_{m,l}$ is the lth root of the derivative of the Bessel function J of order m and A is a coefficient for the main chamber. The difference between the velocity potential for a standing wave and that of a spinning wave is relatively simple. A standing wave is represented by the cos(mθ) term while a spinning wave is represented by a $e^{-im\theta}$ term.

The imaginary frequency, hereafter called λ, is related to the real part of the frequency as follows in equations (7) and (8):

$$\omega = \omega_R + i\cdot\lambda \quad (7)$$

$$e^{i\cdot\omega\cdot t} = e^{i\cdot\omega_R\cdot t}\cdot e^{-\lambda\cdot t} = (\cos(\omega_R\cdot t) + i\cdot\sin(\omega_R\cdot t))\cdot e^{-\lambda\cdot t} \quad (8)$$

The imaginary frequency λ defines the growth or decay behavior of a harmonically oscillating system. If lambda is zero the system will oscillate at a constant amplitude. A value

greater than zero indicates that the equation will grow exponentially with time. A value less than zero indicates exponential decay. In relation to system stabilization, λ values less than zero are desirable. (Note that λ in this equation is different than the λ_{ml} parameter of the Bessel function.)

As a convenience to the reader, the equations used in modeling the potential field within the combustion chamber are presented in Appendix 3 of this text. These equations were used to great effect by Milano et. al.[5] in the development of the DISTCS code. This code can model the stability of a combustion chamber including acoustic cavities, both hub and radial baffles, and other effects.

One of the first analyses of the effect of baffles on acoustic oscillations was performed by Oberg, et al.[6] However, no dissipation mechanism for the baffled chamber oscillations was included in this analysis, so the baffles were found to be destabilizing, rather than stabilizing. Quinlan et al.[7] also predicted that an inviscid baffle structure would have a destabilizing effect.

It is very difficult to develop a physical model for the viscous dissipation at the baffles, as one simply does not know the details of the combustion flow field in that region. Aspects of flow behavior resulting in dissipation such as separation and vortex shedding could be taking place. Without a more complete understanding of the flow field it was decided to be approximated using potential flow theory in the main volume of the combusting flow, and a viscous dissipation model at the boundary layer regions near solid baffle surfaces. Baer and Mitchell[3] developed a streamline-based baffle tip energy dissipation model and included it in an overall combustion stability analysis, predicting a baffle-stabilizing influence.

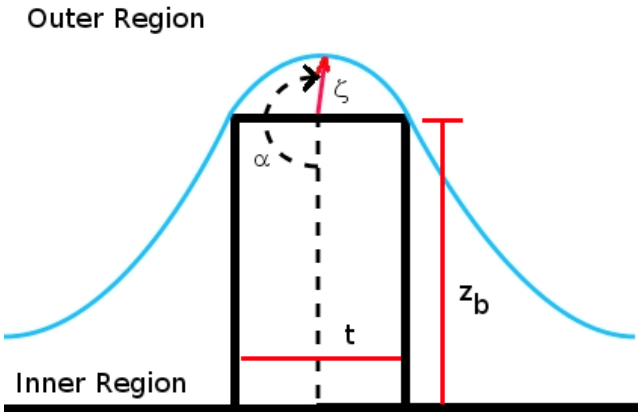

Figure 5: Dividing streamline forming baffle blade tip

To obtain the non dimensional rate of energy dissipation at the baffle tips of the flow field, Mitchell and Baer divided the oscillating flow over the baffles into an inviscid outer region, and a viscous inner region, as shown in Figure 5. The outer solution is obtained using the eigenfunction expansion for the velocity potential which models the combustion chamber at large. The outer solution is then used to drive an oscillatory boundary layer on the tips of the baffle blades. For potential flow around a 360-degree corner of an infinitely thin blade, the streamfunction and velocity potential are:

$$\psi = a \cdot \zeta^{\frac{1}{2}} \cdot \sin\left(\frac{\alpha}{2}\right) \qquad (9)$$

$$\phi = a \cdot \zeta^{\frac{1}{2}} \cdot \cos\left(\frac{\alpha}{2}\right) + k \qquad (10)$$

These potential functions can be found in White.[8] A baffle blade of finite thickness was formed by representing the baffle surface by the edge streamline that passes through the two corner edges of the baffle blade, at $\alpha = \pi/2$ and $3\pi/2$, as indicated in Figure 5. In this way, the

limitation of the potential flow functions in describing infinitely thin baffles could be circumvented. Expressions for the streamfunction, elemental path length, and oscillating velocity were obtained as a function of baffle thickness and the (ζ, α) position along the streamline. The *a* and *k* coefficients in the above equations were found from the outer flow potential solution by solving for both coefficients at the corners of the baffle blade using the potential values at each location. The results are shown below:

$$a = \frac{\phi_1 - \phi_2}{t^{\frac{1}{2}}} \qquad (11)$$

$$k = \frac{\phi_1 + \phi_2}{2} \qquad (12)$$

In this form it is assumed that the locations of φ_1 and φ_2 for the driving potential φ_1 - φ_2 are at mirror angles relative to the centerline from each other. The position at which these values are selected is critical and, in the original analysis, the potential difference was calculated at the baffle tips by choosing the potential values at both corners of the baffle blade. Other formulations of the model have taken the potential difference at other locations, most notably at the injector face next to the baffle by Milano et al.[5] The streamline for the baffle was still the same shape as when the potential difference was located at the baffle tip, however the driving potential could be much larger due to the increased geometric distance between the two sample points. This larger geometric distance leads to greater possibility of large differences between the potential values.

An equation for the effective turbulent viscosity of the oscillating flow in the streamline forming the baffle tip was also developed and incorporated into an energy dissipation expression as potential flow theory makes no allowance for viscosity by its nature. Baer and Mitchell[7] used the following equation (13) to compute the effective turbulence viscosity. In order for the energy dissipation to be integrated along the streamline, the unit path length ds of the streamline was also derived as a function of the angle alpha and is shown in equation (14).

$$v_{eff} = v_{lam} + c_{turb} \cdot \sqrt{U^2 + \varepsilon^2 \frac{u^2}{2}} \qquad (13)$$

$$ds(\alpha) = \frac{t}{4} \cdot \frac{1}{\sin^3\left(\frac{\alpha}{2}\right)} d\alpha \qquad (14)$$

The overall energy dissipation rate in the boundary layer, Equation (16), was computed by first integrating the local energy dissipation flux, Equation (15), along the streamline at a particular cross section of the baffle. The overall dissipation was found by integration along the baffle face using a Gaussian quadrature technique. This procedure was repeated for both the radial as well as the the hub baffle in succession. This dissipation prediction can be matched to experimental data using known λ's computed from pressure decay profiles and varying of the turbulence coefficient parameter c_{turb}.

The Baer-Mitchell baffle energy dissipation model was used to compute the performance of hub baffles by Acker et al.[9], and also used to compute the performance of a combined hub/blade geometry by Milano et al.[5]

$$dE_{diss} = \gamma \sqrt{\frac{v_{eff}(\alpha) \cdot \omega}{2}} u(\alpha)^2 \qquad (15)$$

$$E_{diss} = \int \gamma \sqrt{\frac{v_{eff} \cdot \omega}{2}} u^2 \cdot dS \qquad (16)$$

Further details about the velocity potential eigenfunction solution technique for the baffled combustion chamber are given in Milano et al.[5]

There are some issues with the Baer-Mitchell model that warrant further study. A dimensional analysis of the Baer-Mitchell energy dissipation formula (16) indicates that it is dimensionally inconsistent. The viscosity formula (13) is also dimensionally inconsistent, as it lacks a length scale in the turbulent term. Additionally, any effect that the length of the baffle has

on the system is purely second order as the viscous dissipation which occurs on the sides is ignored. Because of this, it is expected that the model does not couple with the mode shapes quite as well as would be desired. In addition, the dissipation predicted by the baffles does not drop to zero as the length of the baffle is reduced as is expected.

3: Analysis

In order to address the above issues, an improved baffle dissipation model was developed. In this case, a corner-flow streamline allowing for flow detachment at the corners was chosen. The streamfunction and velocity potential equations for a corner-flow streamline are:

$$\psi = \mathrm{a} \cdot \zeta^{\frac{2}{3}} \cdot \sin\left(\frac{2\alpha}{3}\right) \qquad (17)$$

$$\phi = \mathrm{a} \cdot \zeta^{\frac{2}{3}} \cdot \cos\left(\frac{2\alpha}{3}\right) + k \qquad (18)$$

Equations 17 and 18 demonstrate that the overall functions are the same except a factor of 2/3 has been introduced where previously a 1/2 was used. A graphical representation of the streamline separating at the corner for the time period when the oscillating flow is moving from left to right is shown below in Figure 6. The major benefit of approaching the streamline in this way is that the resulting fluid path is much more consistent with what would be expected to be physically occurring. In addition, by the very nature of the streamline the length of the baffle must be included. Since the flow is oscillating, it will also be moving to the left for half the oscillation period, and the streamline will be assumed symmetric about the centerline of the baffle when viewed at the extrema of the period of its oscillation. Care must be taken however in the way that the dissipation over this period of oscillation is taken as the potential in the combustion chamber is modeled in the frequency domain. In the same way as the Baer-Mitchell model, the outer

region above the streamline is modeled as inviscid flow using the potential values from the eigenfunction solution, and the region below the streamline is modeled as viscous flow.

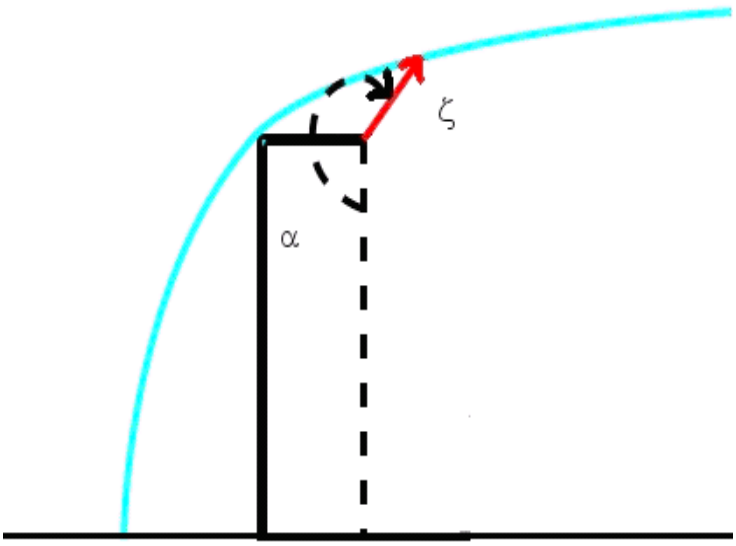

Figure 6: Corner separation streamline

Expressions for the streamfunction value, elemental path length dS, and oscillating velocity u along the edge streamline shown in Figure 6 were obtained as a function of baffle thickness and the (ζ, α) position along the streamline. The equation for the length of ζ as a function of α is given in equations (19) and (20) where C is a constant used to simplify the expression of ζ.

$$C = \left[\frac{\sqrt{3}}{2} \cdot \left(\frac{t}{2}\right)^{\frac{2}{3}}\right] \tag{19}$$

$$\zeta(\alpha) = \left[\frac{C}{\sin\left(\frac{2}{3} \cdot \alpha\right)}\right]^{\frac{3}{2}} \tag{20}$$

The a and k coefficients in equations were found using the outer flow potential solution, as shown in equations 21 and 22.

$$a = \frac{\phi_1 - \phi_2}{\zeta(\alpha_1)^{\frac{2}{3}} \cdot \cos(\frac{2}{3} \cdot \alpha_1) - \zeta(\alpha_2)^{\frac{2}{3}} \cdot \cos(\frac{2}{3} \cdot \alpha_2)} \quad (21)$$

$$k = \phi_1 - a \cdot \zeta(\alpha_1)^{\frac{2}{3}} \cdot \cos(\frac{2}{3} \cdot \alpha_1) \quad (22)$$

In an effort to further remove any time dependance from the solution the selection of the driving potential φ_1 and φ_2 is of large importance. For the purposes of this analysis it will be assumed that the potential in the combustion chamber is harmonic in its oscillation over time and can be described as a sinusoidal function. The baffle blade is assumed to only dissipate energy when the potential at the base of the blade is larger than at the tip, i.e. a driving flow field. The locations of the potential are shown in Figure 7. This figure demonstrates the assumed streamline at the two maxima of the oscillation. While the oscillation is occurring from $\omega t = 0$ to π the dissipation is assumed to occur between φ_a and φ_{zb}. The dissipation is then assumed to switch to the opposite side of the baffle blade where $\omega t = \pi$ to 2π and the dissipation occurs between locations φ_b and φ_{zb}. Assuming that the magnitude of these potentials varies sinusoidally, the total potential difference over one period can be described by the following function:

$$\Delta\phi = \int_0^{\pi} (\phi_a - \phi_{zb}) \cdot \sin(x)\, dx + \int_{\pi}^{2 \cdot \pi} (\phi_b - \phi_{zb}) \cdot \sin(x)\, dx \quad (23)$$

In this case φ_a and φ_b are, from the formulation of the parameter a in equation (21), φ_1 for each half of the period respectively. φ_2 is represented by φ_{zb}. Integrating this function yields an expression for the potential difference during a full period of oscillation.

$$\Delta\phi = 2\cdot\left(\phi_a - \phi_b\right) \qquad (24)$$

This result implies that the base of the baffles is the most physically accurate location for both φ_1 and φ_2. In addition, it also adds a factor of two to the value of the parameter a in equation (21).

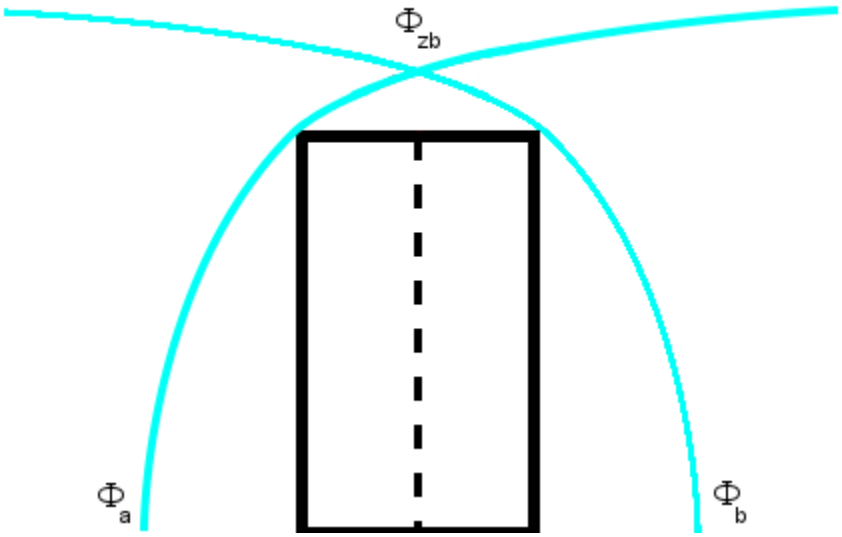

Figure 7: φ selection locations

By manipulation of the ζ, a and k functions, the streamline and oscillatory velocity terms can be derived as shown in equations (25) and (26).

$$ds(\alpha) = \sqrt{\frac{C}{\sin^5(2\frac{\alpha}{3})}} \qquad (25)$$

$$u(\alpha) = \sqrt{\frac{\frac{4}{9}\cdot a^2 \cdot \sin(\frac{2}{3}\cdot\alpha)}{C}} \qquad (26)$$

The viscosity model used in the corner flow model is different than the Baer model. It should be noted that turbulence models using an eddy viscosity concept have a local velocity scale and a local length scale to characterize the local eddy viscosity ν. For example, the eddy viscosities of boundary layer flow are assumed to be proportional to the product of a local velocity and length. In this corner flow analysis we choose a local fluctuating velocity $(U^2 + u^2)^{1/2}$ as the local velocity scale, and the baffle height z_b as the local length scale. Owing to the physical difference between these two models it does not seem reasonable to continue referring to the turbulence coefficient of the corner-flow model as c_{turb}. Therefore, the coefficient of turbulence for the corner-flow model will be called c_1 since it is used in a different viscosity formulation. The effective viscosity equation is as follows:

$$\nu_{eff} = \nu_{lam} + c_1 \cdot z_b \cdot \sqrt{U^2 + u^2} \qquad (27)$$

The rate of energy dissipation in the volume below the dividing streamline can be determined by integrating the corner flow normal to the streamline, and then integrating along the streamline and baffle face, as indicated by Equation (28):

$$E_{diss} = \int \frac{Power}{Vol}\, dV = m \int \int_{\delta_1}^{\delta_2} \left(\frac{du}{dy}\right)^2 dy\, \mathrm{dS} \qquad (28)$$

For a streamline oscillating at a velocity with amplitude of u and frequency ω, an equation for the fluid velocity gradient *du/dy* a distance y from the streamline is given by Equation (29a). This expression can be derived from the solution for a plate oscillating in fluid. This velocity gradient is averaged over one oscillation period. To do this, the function is integrated from zero to 2π and then divided by 2π. Performing this integral of the du/dy term and then integrating it from $\delta_1 = 0$ to $\delta_2 = \delta$ as shown in equation (29) yields:

$$\frac{du}{dy} = u\sqrt{\frac{\omega}{2\nu}}\sin\left(\omega\cdot t-\left(\frac{\omega}{2\cdot\nu}\right)^{\frac{1}{2}}y\right) \qquad (29a)$$

$$\tau=\frac{2\cdot\pi}{\omega}$$

$$\frac{Average}{period}: \quad \frac{1}{\tau}\int_0^{\tau}\int_0^{\delta}\sin\left(\omega\cdot t-\sqrt{\frac{\omega}{2\cdot\nu}}\cdot y\right)^2 dy\,dt$$

$$A=\cos(4\cdot\pi)-1$$

$$B=\left(2\cdot\sin\left(\delta\cdot\sqrt{\frac{\omega}{2\cdot\nu}}-2\cdot\pi\right)^2-2\cdot\sin\left(\delta\cdot\sqrt{\frac{\omega}{2\cdot\nu}}\right)^2\right)$$

$$\frac{Average}{period}: \quad \frac{\delta}{2}+\frac{1}{16\cdot\pi\cdot\sqrt{\frac{\omega}{2\cdot\nu}}}\cdot(A+B)$$

$$\frac{1}{16\cdot\pi\cdot\sqrt{\frac{\omega}{2\cdot\nu}}}\cdot(A+B)=0$$

$$\frac{Average}{period}=\frac{\delta}{2}$$

$$\frac{du}{dy}=u\cdot\sqrt{\frac{\omega}{2\cdot\nu}}\cdot\frac{\delta}{2} \qquad (29b)$$

The penetration depth δ can either be directly calculated as the distance from the baffle or the streamline or, to save on computation power, the penetration depth can be approximated. From scale analysis, the penetration depth δ of the oscillation scales as:

$$\delta \approx \sqrt{\frac{\nu_{eff} \cdot 2\pi}{\omega}} \qquad (30)$$

Upon substitution of Equations (29b) and (30) into Equation (28), the rate of energy dissipation in the viscous layer at an angular location α along the streamline is given by Equation (31), and the total rate of energy dissipation is found by integrating over the baffle tip surface area as shown in Equation (32):

$$dE_{diss} \approx \frac{\rho \cdot u^2 \cdot \omega \cdot \delta}{2} \approx \frac{\rho \cdot u^2}{2} \cdot \sqrt{\frac{\nu_{eff} \cdot \omega}{2}} \qquad (31)$$

$$E_{diss} = \int \frac{\rho \cdot u^2}{2} \cdot \sqrt{\frac{\nu_{eff} \cdot \omega}{2}} \cdot ds \qquad (32)$$

As can be seen, the resulting integral form is essentially identical to that is typically used to compute the acoustic power loss at a surface, and is similar in structure to the Baer-Mitchell model, see Equation (16), with the difference being the incorporation of the density term ρ instead of the specific heat term γ. Another observation that may be made is that due to the oscillations penetrating into the fluid at a distance δ the corner-flow model views the energy loss as being a volumetric effect as opposed to a surface level occurrence. This difference in the conceptual nature of the model is also another indication that the turbulence coefficients are not the same between the two models.

4: Results

4.1: Comparison of Local Energy Dissipation Flux

To compare these two dissipation models, we first look at a simple example of the energy dissipation per unit area along a streamline over a baffle with fixed driving potential difference. The following plots compare the rate of energy loss of the corner flow model compared to the Baer-Mitchell model. Parameters such as local velocity, elemental path length, effective viscosity, and local energy dissipation rate are computed and compared as a function of the local angle α for each model. In this example, it is assumed that the velocity potential difference, $\varphi_1 - \varphi_2$, across the baffle in the combustion chamber is held constant at 0.5 - 0.2 = 0.3. In this manner the two models are compared directly and the dependance upon the outer flow potential φ can be negated for the moment. A value of c_{turb} and c_1 equal to 1.0 was chosen for these calculations. The baffle blade geometry was chosen with a nondimensional length of 0.15 and thickness of 0.05. For the Baer-Mitchell model, a value for ε of 0.1 was used which is a value used in test cases previously. As shown in equation (27) this parameter has been removed from the corner-flow model. The removal of this value is expected to reduce the value of c_1 slightly required in the corner model to achieve a similar dissipative effect as the Baer-Mitchell model.

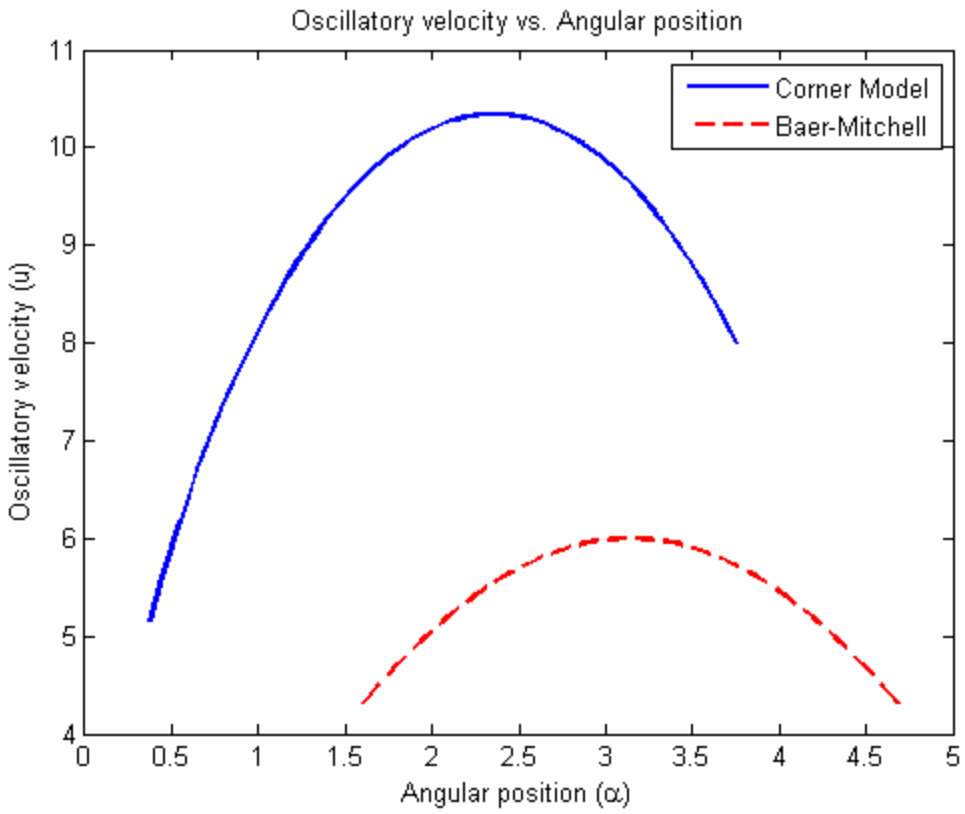

Figure 8: Comparison of oscillating velocity profile

The change in the oscillatory velocity along the streamlines for the Baer-Mitchell and the corner flow are given in Figure 8. The Baer-Mitchell line is plotted from one baffle corner tip to the opposite corner, from $\alpha = \pi/2$ to $\alpha = 3\pi/2$, while the corner-flow model is plotted from the base of the baffle blade to the value of α which corresponds to the streamline being located just above the opposite corner. In order to find this value of α, an iterative process was required. The basic shape of both velocity profiles is very similar, with different locations of a maximum oscillatory velocity. Figure 9 plots the variation of the non-dimensional effective turbulent viscosity along the streamlines for both models. The corner-flow turbulent viscosity is about a factor of three larger, and has more streamline position dependence than the Baer-Mitchell model. This is a function of

the added length scale and the removal of the pressure oscillation term ε in addition to several numerical coefficients resulting from equations (24) and (29a).

In Figure 10, the energy dissipation flux, dE_{diss}, is plotted as a function of streamline location for both models, using Equation (15) for the Baer model, and Equation (31) for the corner-flow model. The corner-flow energy dissipation is much larger in this configuration, and again has more streamline position dependence.

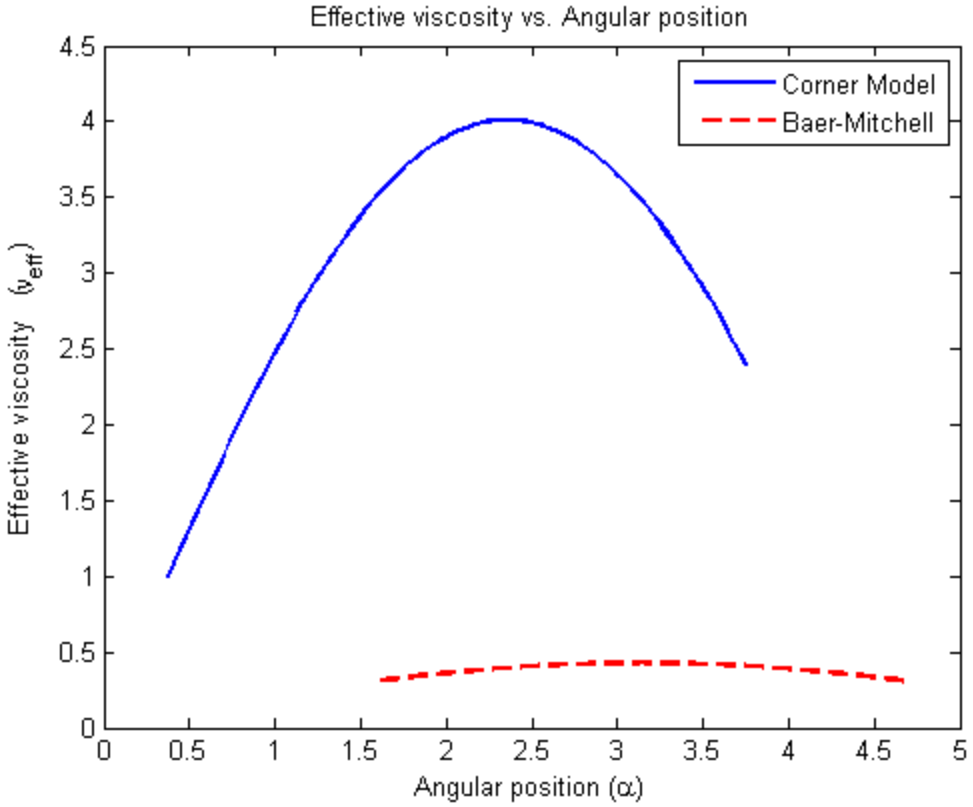

Figure 9: Effective viscosity comparison

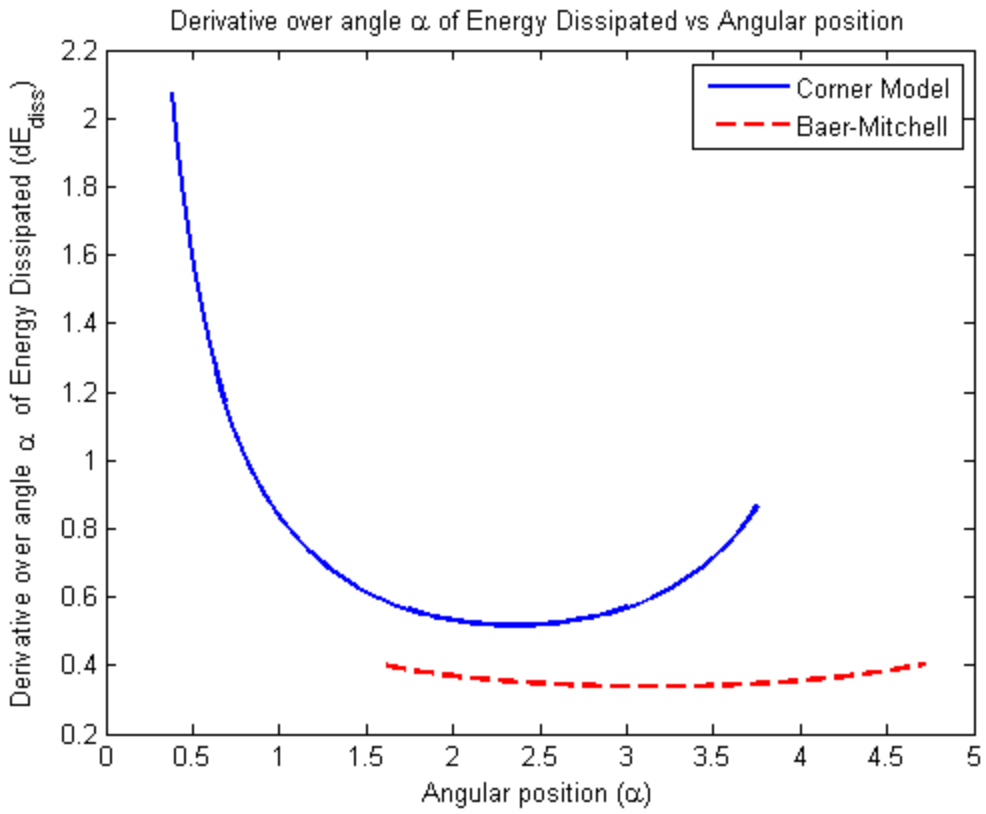

Figure 10: Local energy dissipation comparison

4.2: Energy dissipation rate in representative test engine

We now compute the baffle energy dissipation rate for a hub/blade baffle configuration in a representative test engine. The representative test engine of Acker[7] which described a combustion chamber with a hub only is utilized. Modifications to this model by Milano[8] have been included for study in this paper. This is so that the chamber geometries contained within this paper are consistent with a test case which has been utilized in past papers. The engine has a chamber with a non-dimensional length of 2.5, a hub radius of 0.4, and five evenly spaced radial blades with a non-dimensional length of 0.15, and non-dimensional thickness of 0.05. On this section the turbulence coefficient was held constant at c_1 =1.00, for the purposes of this paper, whenever the Baer-Mitchell or Milano models are used, a value of 5.0 for c_{turb} will be used unless

otherwise specified. This value is chosen because it is the default setting in DISTCS. Unless otherwise specified, no cavities are used. The reason for this decision was to show the effects of the baffles alone without any additional dissipation by the cavities.

The overall baffle energy dissipation rate E_{diss} is found by integrating the energy dissipation rate per unit area, dE_{diss}, over the hub/blade face area in the radial and azimuthal directions, using Gauss quadrature. The independent variables are the acoustic mode shape, baffle length z_b, and baffle thickness t relative to baseline values. The acoustic frequency for a particular mode is dependent on the baffle length, and decreases a small degree as the baffle length is increased.

Note that the incorporation of the energy dissipation model into a combustion stability calculation introduces a stronger dependence on the mode shape than is possible with the simple plots shown in the previous section which were calculated with constant $\varphi_1 - \varphi_2$. In a combustion stability computation, the values of φ_1 and φ_2 used to calculate the local values of the streamline variables a and k at each (r, θ) location along the surface of the baffle are different. The potential at any given location is a function of the mode which has been chosen by the user. In this way, the model is coupled to the existing mode in the combustion chamber in a way that was not possible with the simple equation models before. The energy dissipation rate becomes dependent on the acoustic mode existing in the chamber, since the value of the variables a and k at a given (r, θ) location on the baffle face are directly proportional to the local values of $\varphi_1 - \varphi_2$ at that location for a given engine geometry and acoustic mode. The value of is shown in Figure 11 for the 1R and in Figure 12 for the 1T mode demonstrating the dramatic difference that exists in the potential values. This $\varphi_1 - \varphi_2$ is computed across the base of the baffle blade. The location from the injector face where this potential difference is calculated is called z_{match}.

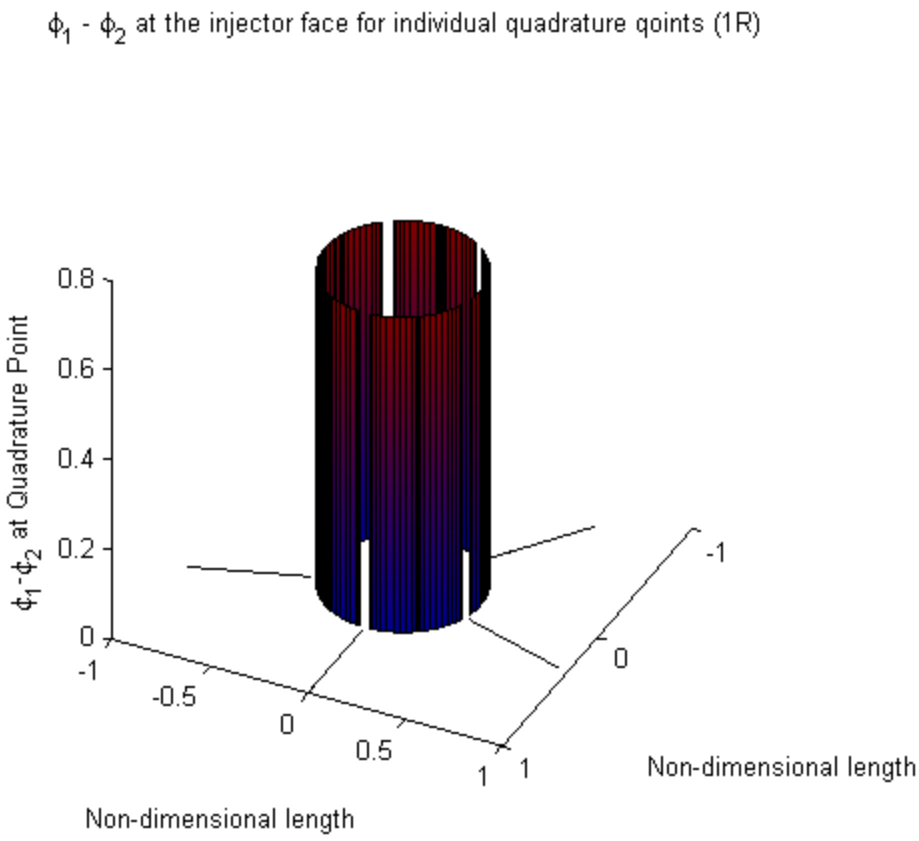

Figure 11: φ_1 - φ_2 at the injector face for the 1R mode.

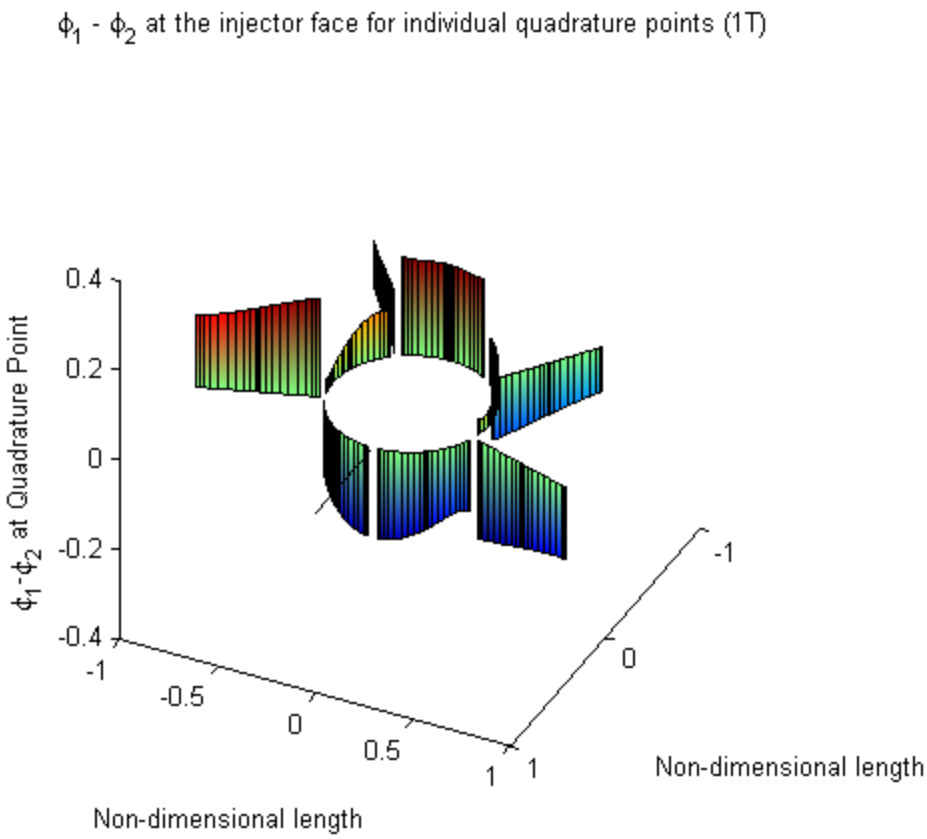

Figure 12: φ_1 - φ_2 at the injector face for the 1T mode

A direct comparison of the difference compared to φ_1 - φ_2 across the baffle tip is also warranted. As stated before, the Baer-Mitchell model was originally intended to use the potential difference across the baffle tips. In Figure 13 and 14, the overall shape remains reasonably consistent compared to the potential difference computed the base. Separate sections tend to blend together more than in the baffle base potential difference. The magnitudes between the two are significantly different indicating that the corner-flow model will be utilizing a much larger change in potential, than tip difference of the Baer/ Mitchell model.

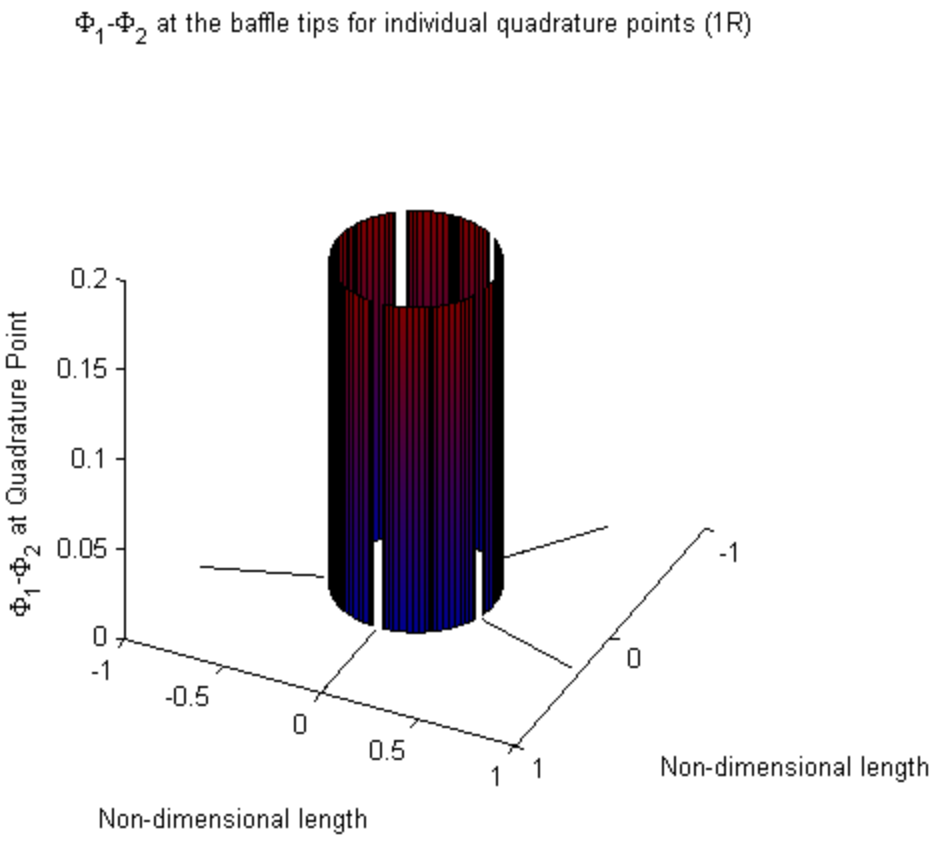

Figure 13: Baffle tip φ_1 - φ_2 1R mode

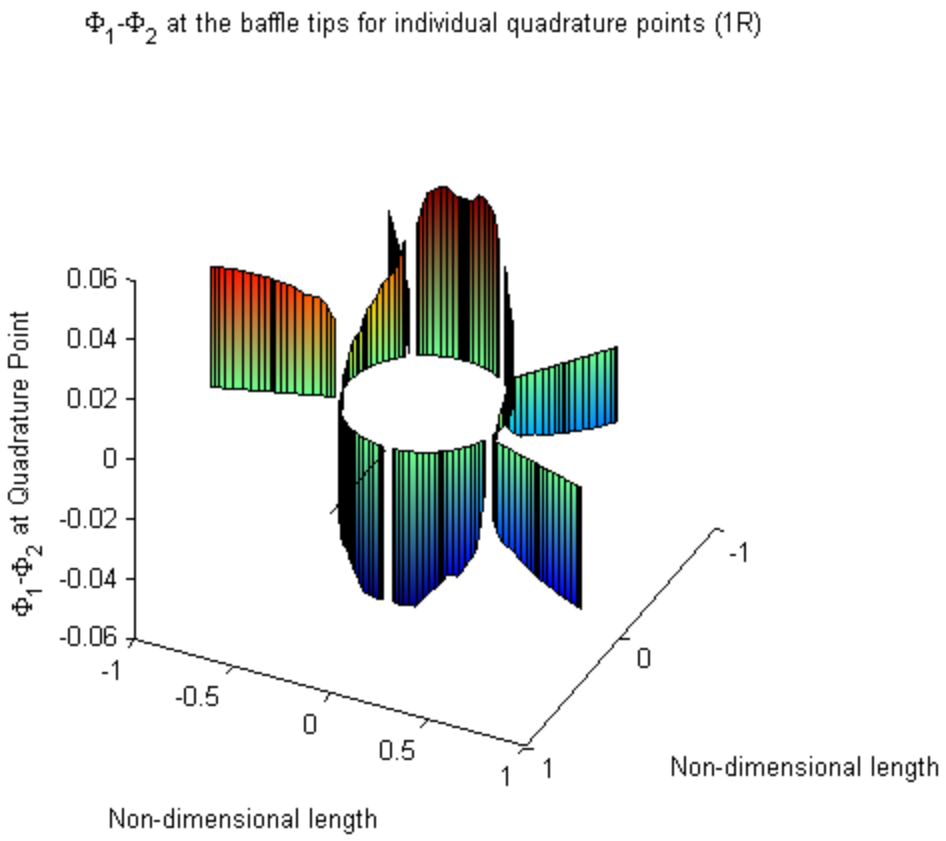

Figure 14: Baffle tip φ_1 - φ_2 1T mode

These figures demonstrate clearly how the potential difference across the baffle blade varies significantly with the location of z_{match}. To understand the effects of locating the potential difference at different locations a plot of the pressure is useful. This pressure can be calculated from the potential φ using equation (33).

$$P = -\gamma \cdot \rho \cdot \left(i \cdot \omega \cdot \phi + \bar{u} \cdot \frac{\partial \phi}{\partial z} + \phi \cdot \frac{\bar{Q}}{\bar{\rho}} \right) \qquad (33)$$

Figures 15 and 16 clearly demonstrate the differences between the 1R and 1T modes. Both of these plots are (r,θ) plots indicating pressure profiles axially and radiallly at θ values of 0

and π. In these figures the injector face is located to the right while the nozzle is located to the left of the image. The 1R mode seen in Figure 15 appears to have a significant pressure increase in the hub as opposed to the lower potential in the baffle compartments. This forcing pressure would be expected to drive large amounts of dissipation for this mode. The small breaks in the pressure plot are due to the location of the hub baffle. The 1T mode in Figure 16 predicts much less pressure differential between the hub and the baffle compartments. This is not unexpected given the evidence of the potential differences in Figures 12 and 14.

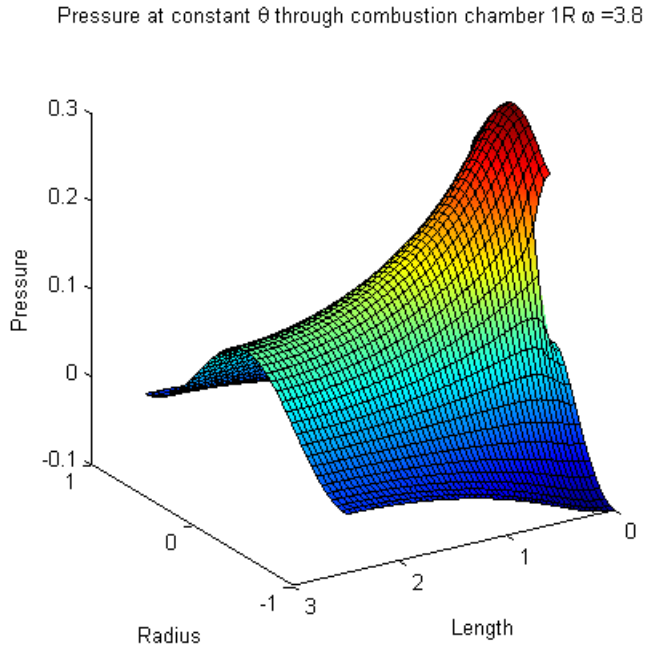

Figure 15: Axial pressure distribution 1R mode

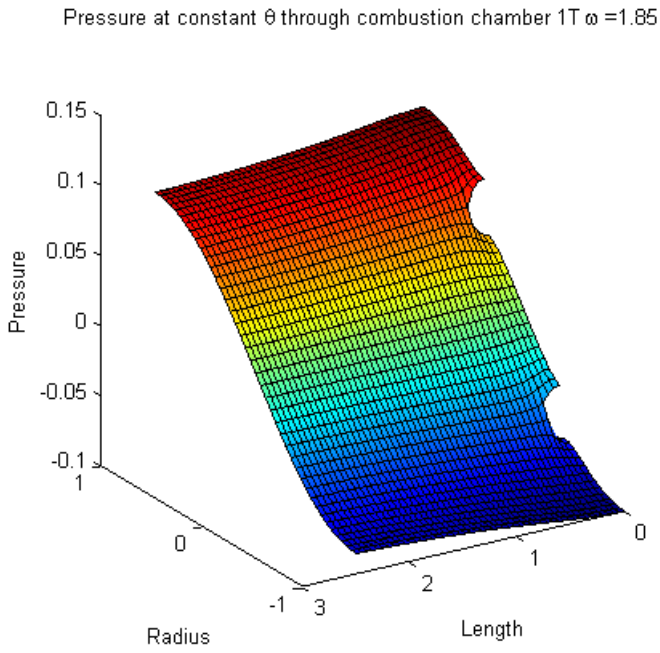

Figure 16: Axial pressure distribution 1T mode

To determine the local distribution of the energy dissipation across the baffle blades for the corner-flow model, a series of plots showing the dissipation at the quadrature points for the 1R as well as the 1T mode are provided. The values of φ_1 and φ_2 were selected at the injector face as in Figures 11 and 12. Attention should be paid to the magnitude of the dissipation with the 1R mode showing dissipation values nearly 20 times larger than the tangential modes. Most noticeable is that the dissipation is proportional to the difference in potential which is most evident in the 1R mode. This is to be expected given the method with which the streamline was formed but it is evidence that the model is coupling into the mode shape as desired.

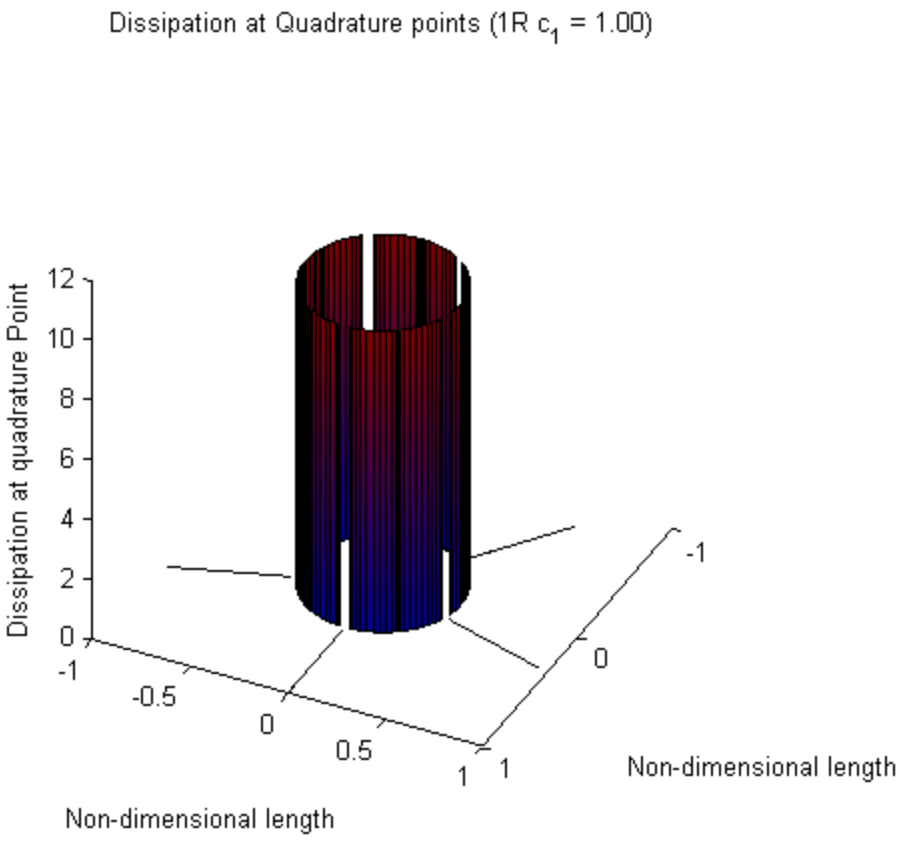

Figure 17: Corner flow model dissipation for 1R

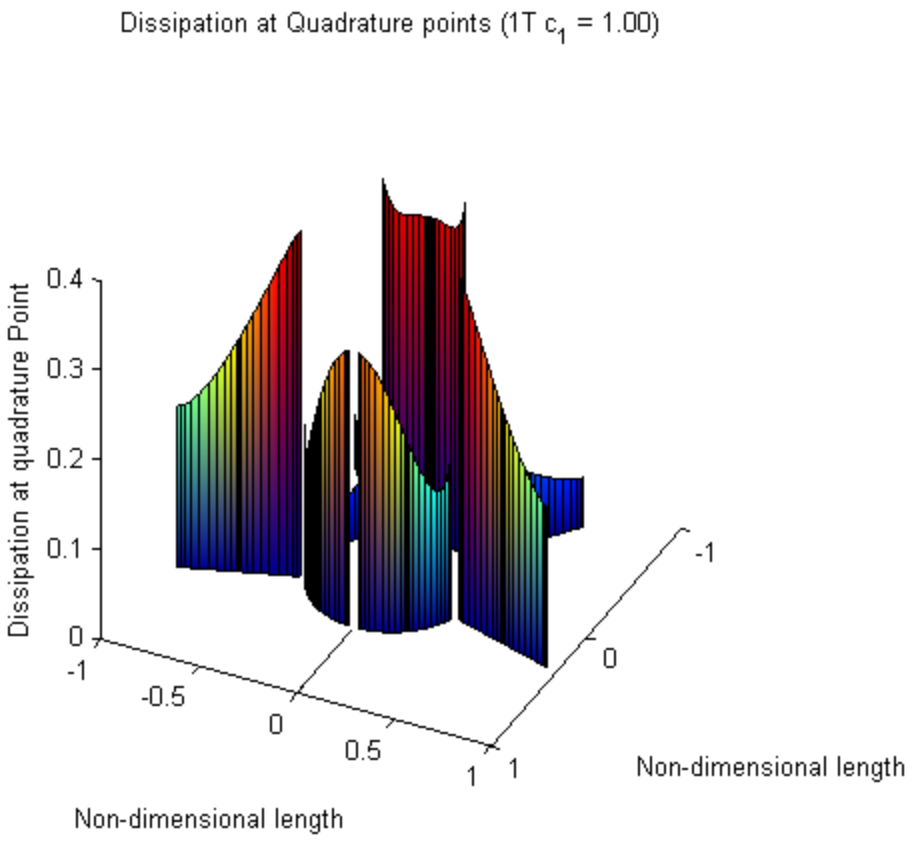

Figure 18: Corner flow model dissipation for 1T

The following figures are a comparison of the dissipation profiles generated by the Baer-Mitchell model with the potential difference taken across the baffle blade at the injector face. From this point on in this section, all plots and figures referring to Baer-Mitchell uses a potential difference calculated at the injector face. This is to provide a more direct comparison between the models. These plots demonstrate that, again, the model has coupled into the potential profiles correctly and appears to be a proportional scaling of the magnitude.

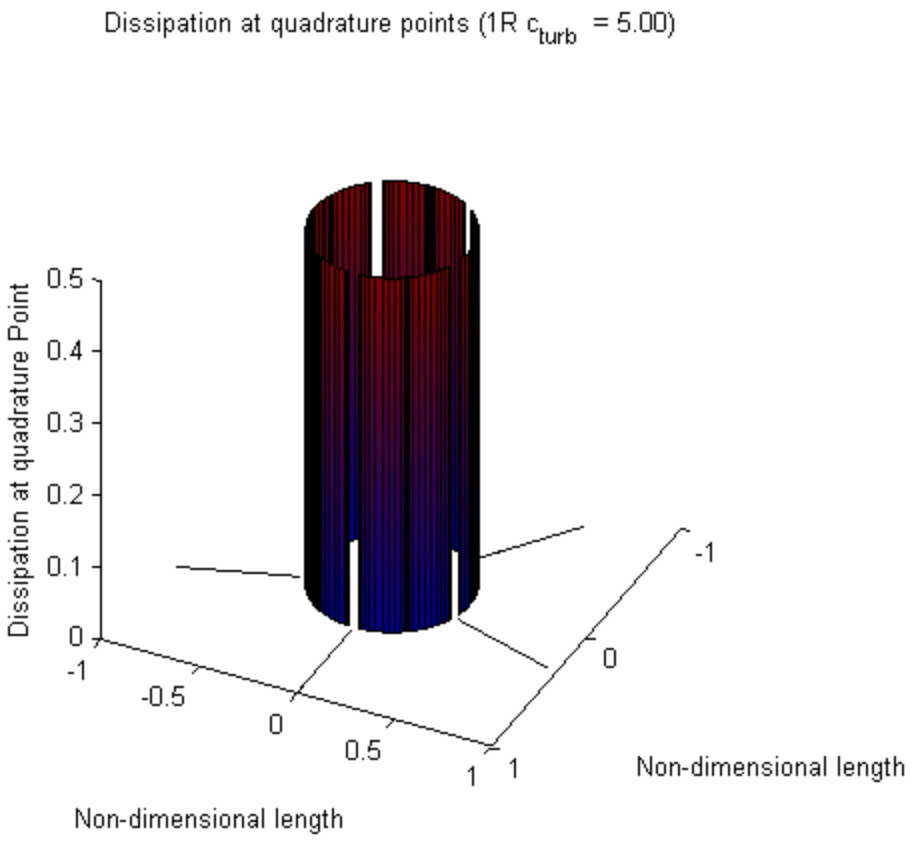

Figure 19: Baer-Mitchell Dissipation 1R

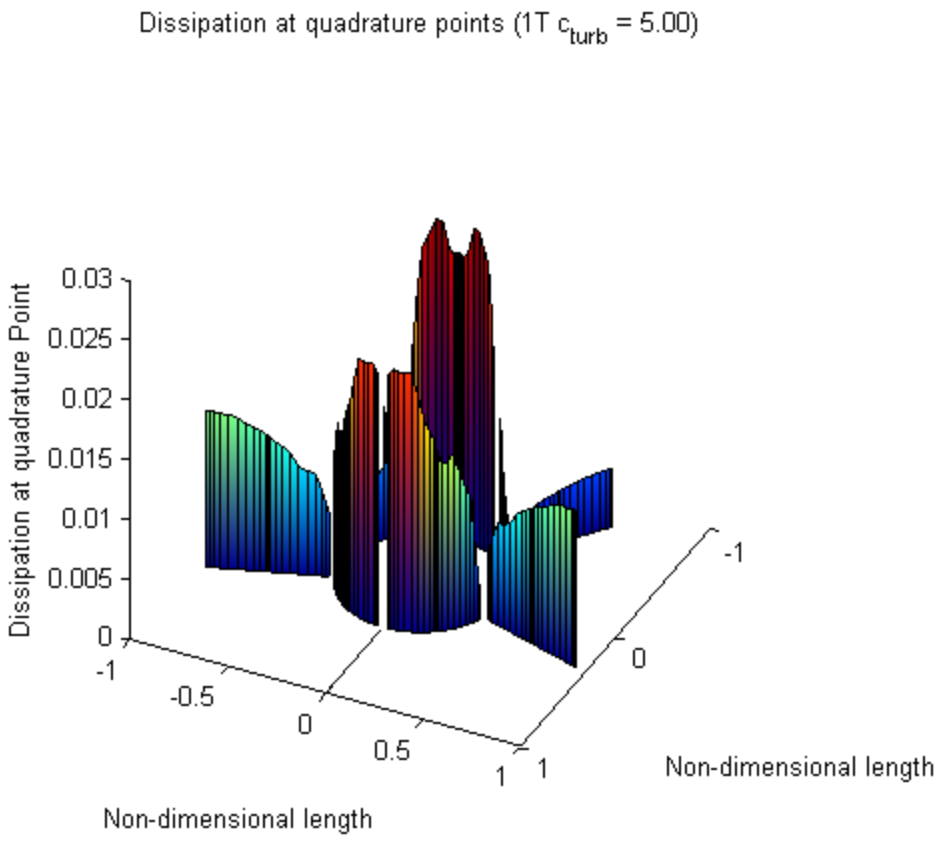

Figure 20: Baer-Mitchell Dissipation 1T

4.3: C_1 variation study

The corner flow model turbulence coefficient c_1 can be determined by matching with test data. Milano found that values of c_{turb} of the order of 5-50 would be appropriate for the Baer-Mitchell model. These values are, essentially, arbitrary constants and large variation between models is to be expected. Using the test engine case it was clearly demonstrated that the corner-flow model carries increased sensitivity to c_1 so that one would expect c_1 and c_{turb} to be different.

In order to match the value of c_1 to a decay rate λ, a method of matching the minimum |CRES| values predicted by the code was used. Initially, the stability of clean chamber was computed with λ = 0 to give a baseline. A range of frequencies spanning the acoustic frequency were used. For the 1R, ω was varied from 3.0 to 4.5. For the 1T ω was varied from 1.0 to 2.5. The damping was then incremented from λ = 0.05 to 0.20 and the minimum resulting |CRES|

values were noted. These are the horizontal 'clean chamber' lines on the plots. Then the stability code was run with baffles with different values of c_1 using the Acker/Milano engine and the minimum |CRES| values from a |CRES|-ω plot were identified. The results of these studies are presented in the following figures.

The |CRES| vs c_1 curves for the corner flow model is presented in Figure 21 for a 1R and Figure 22 for a 1T along with the constant |CRES| lines for the clean chamber with varying decay parameters. The intersection of the corner flow line with the clean chamber lines gives the value of c_1 value that would correspond to the clean chamber decay λ. For example, for a decay parameter λ = 0.10, the equivalent c_1 = 0.005.

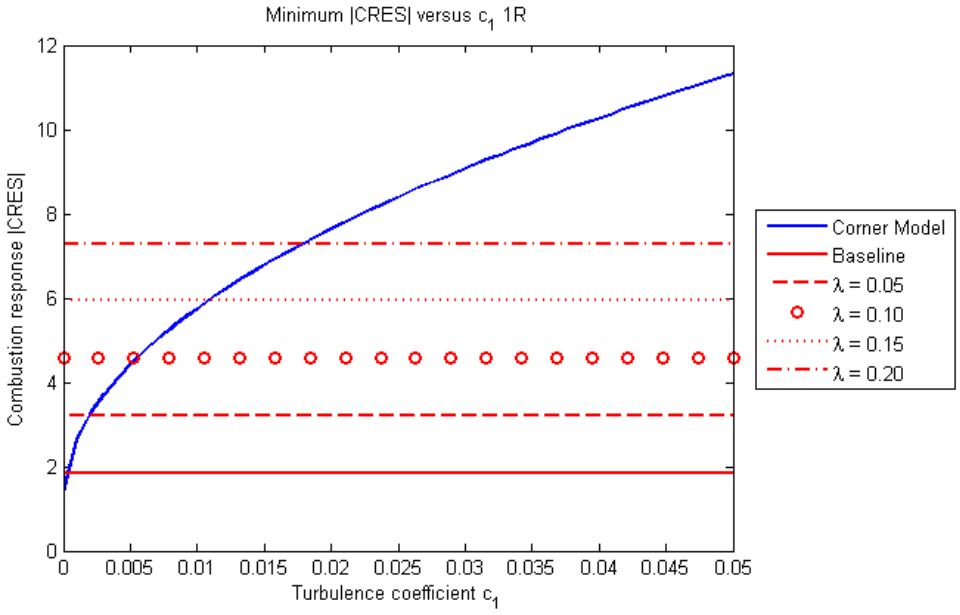

Figure 21: Minimum |CRES| as a function of c_1 from 0 to 0.05 (Corner flow model 1R)

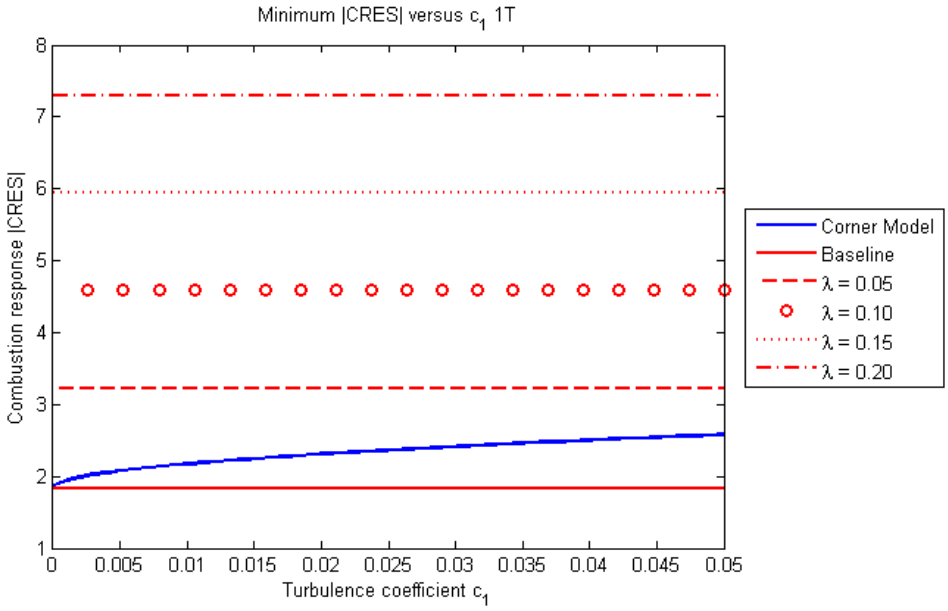

Figure 22: Minimum |CRES| as a function of c_1 0 to 0.05 (Corner flow model 1T)

The minimum |CRES| values predicted by the Baer-Mitchell model for larger of c_{turb} are presented in Figures 23 and 24. The increased values of c_{turb} when compared to c_1 are likely a combination of the length scale in the viscosity term as well as the removal of the ε term in addition to integration constants coupled with the factor of two added to equations (21) and (22) as stated before. Figures 23 and 24 demonstrate the predicted minimum |CRES| values for both the 1R and the 1T mode for the Baer/ Mitchel model.

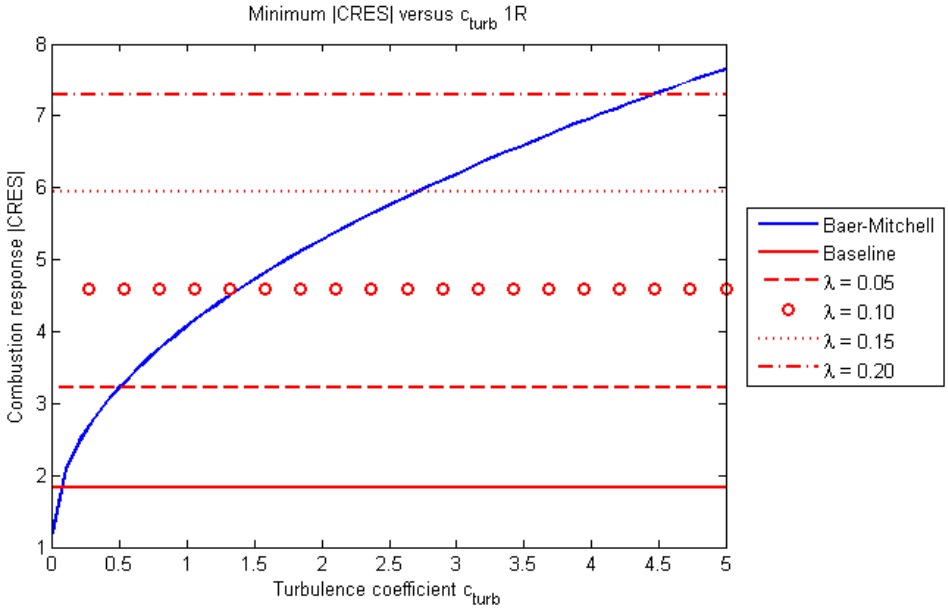

Figure 23: Minimum |CRES| as a function of c_{turb} from 0 to 5 (Baer-Mitchell 1R)

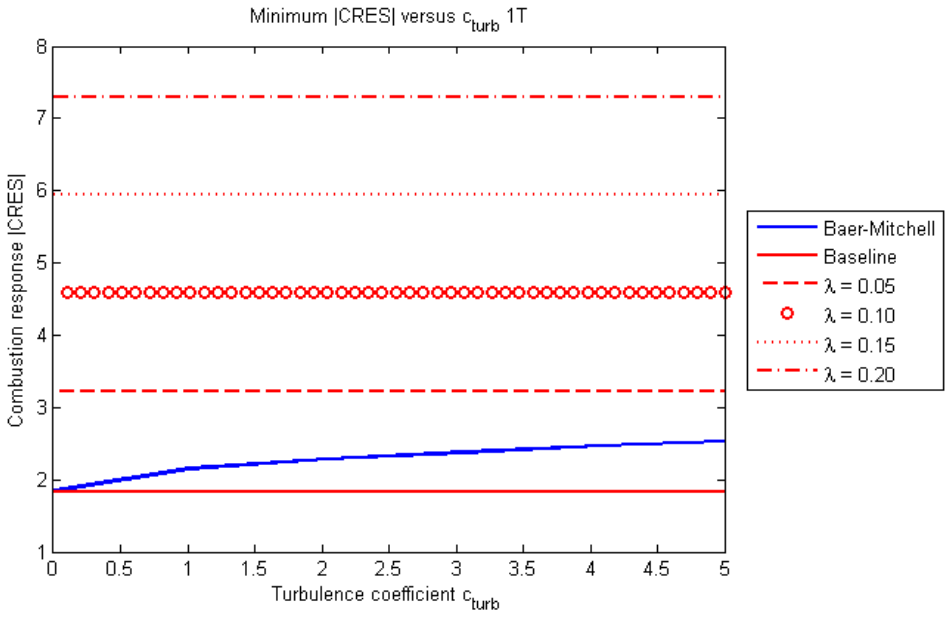

Figure 24: Minimum |CRES| as a function of c_{turb} 0 to 5 (Baer-Mitchell model 1T)

Using Figures 21 through 24 the value of c_1 which most closely matches the default value of c_{turb} of 5.0 can be calculated. For c_{turb} = 5.0 from Figure 23 the |CRES| value for the Baer-Mitchell model for the 1R is approximately 7.5 from Figure 23 and from Figure 24 the |CRES|

value for the 1T mode is approximately 2.5. From Figures 21 and 22 this corresponds to c_1 values of 0.02 and 0.04 respectively. Taking the average of these two values yields a value of 0.03. Therefore, to accurately compare the models a c_1 value of 0.03 will be utilized.

4.4: Z_{match} variation study

Figures 25-28 demonstrate the dependance of the minimum |CRES| on the location of z_{match} varying from the injector face to the baffle blade tip. Again, z_{match} is the z location where the driving potential difference $\varphi_1 - \varphi_2$ across the baffle is calculated. There is a location where the model predicts the maximum dissipation to occur. This point is between the injector face and the tip of the baffle. The maxima is directly due to the interaction of the length scale in the viscosity model and the cosine terms in the formulation of the 'a' coefficient. The coupling of these variables defines the slope of the minimum |CRES| line. This occurrence implies that, as a design tool, it might be useful to be able to use a variable z_{match}. This additional variable in conjunction with c_1 could make it possible to fine tunie the response of a simulated engine geometry to test data. While the base of the baffle blades is perhaps the most physically correct region for the potential difference to be calculated, varying the location of z_{match} could allow for factors outside of the scope of the model to be accounted for. Of note is that the value of c_1 causes the minimum |CRES| value to asymptotically approach the c_1 equal to zero case when the position of z_{match} is at the injector face. The 1T and 1R modes seem to have the same general shape with varying overall magnitudes.

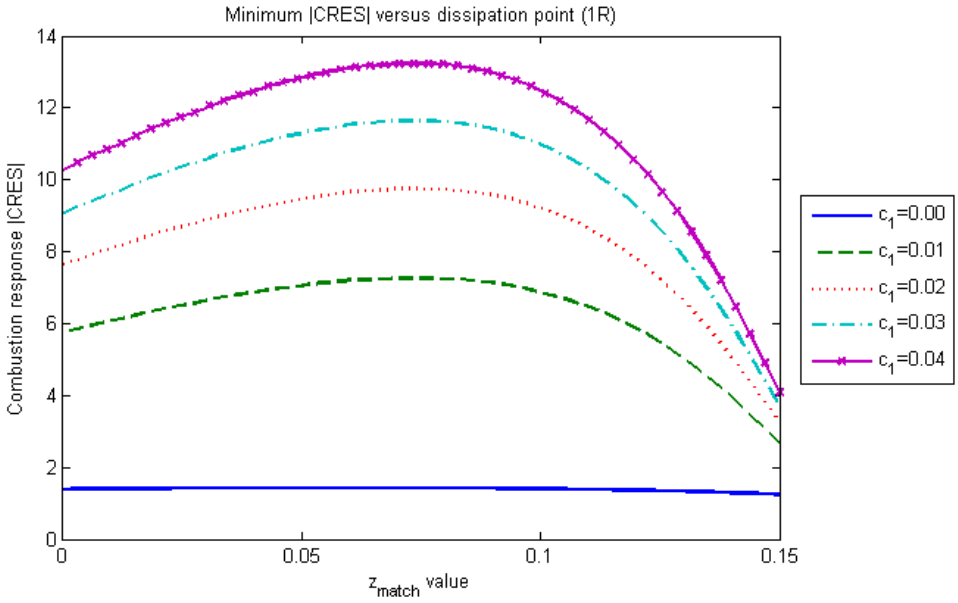

Figure 25: Minimum |CRES| value variation as z_{match} changes 1R

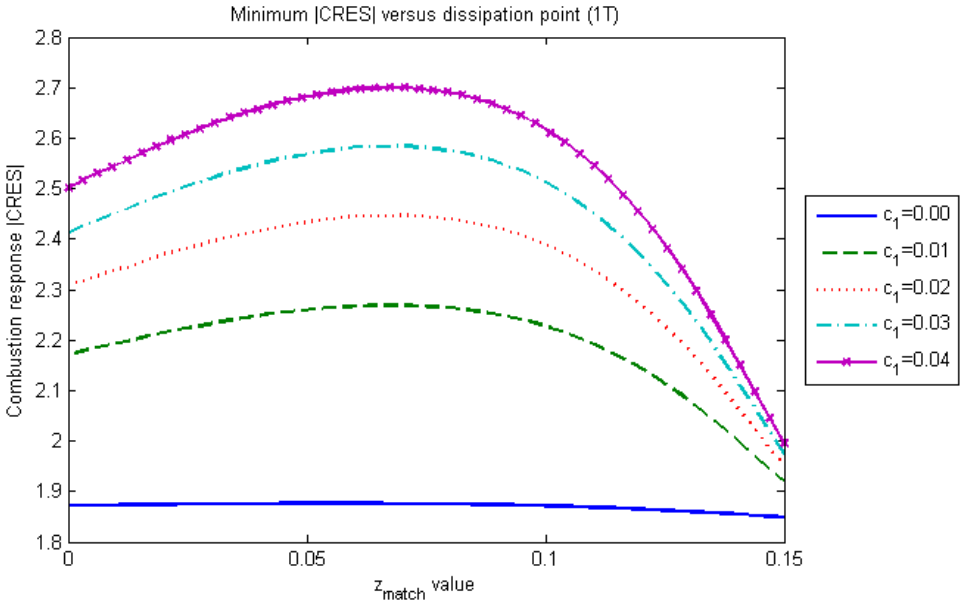

Figure 26: Minimum |CRES| value variation as z_{match} changes 1T

The Baer-Mitchell model appears to be similarly sensitive to the variation of z_{match} for a given c_{turb} and similar value of c_1. The location of the maximum predicted dissipation appears to occur, for this particular geometry, near the tip of the baffle as opposed to the corner-flow model

which predicted the dissipation more towards the middle of the baffle blade. This is evidence that the corner dissipation model has a greater amount of coupling with the wave shape and surrounding baffle structure than the Baer-Mitchell model as the velocity potential appears to have a greater effect on the predicted dissipation than the formulation of the equations in the model.

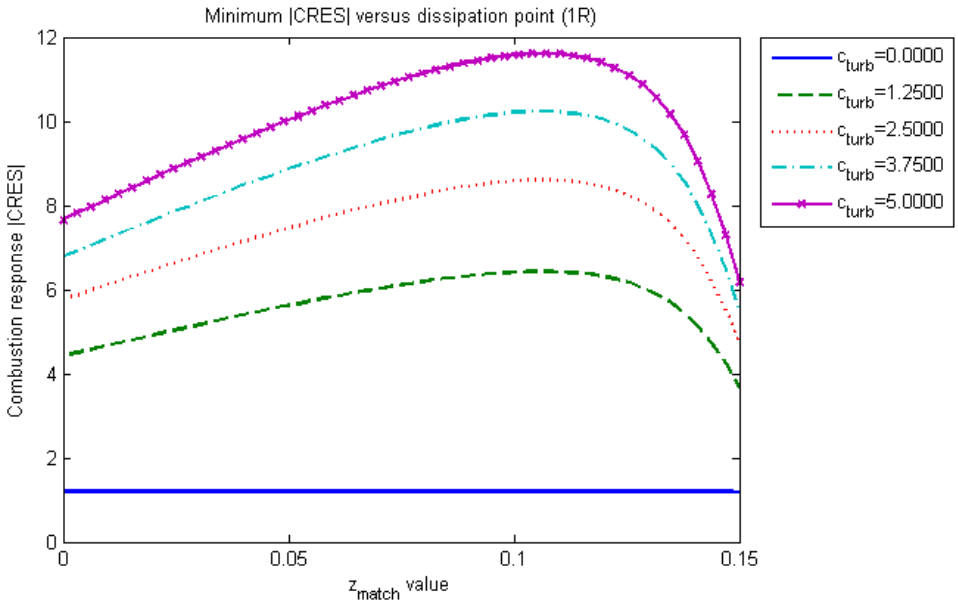

Figure 27: Minimum |CRES| value variation as z_{match} changes 1R Baer-Mitchell

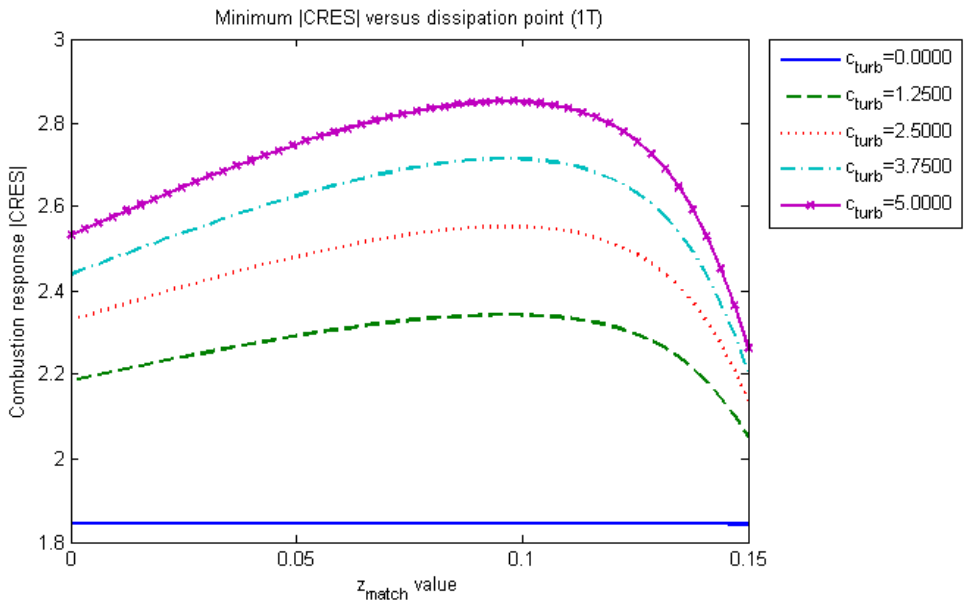

Figure 28: Minimum |CRES| value variation as z_{match} changes 1T Baer-Mitchell

In addition to the location of z_{match} the distance from the surface of the baffle blade at which the potential is obtained is also of importance. In the Baer-Mitchell model and all previously shown plots, the location of matching has been against the surface of the baffle. An alternate method is to place the matching location at the distance away from the baffle blade the streamline is predicted to be as shown in Figure 7. As a means of comparing the differences in dissipation between the two matching locations, plots have been provided varying z_{match} with the minimum |CRES| value plotted for each case are shown in Figure 29. The plots are using a c_1 value of 1.250. At each point, the distance from the baffle blade to the streamline which corresponded with each individual value of z_{match} was computed. As can be seen, the minimum |CRES| value is increased, though only slightly. The difference appears to increase slightly as the location of z_{match} moves closer to the end of the blade before the lines intersect just before the tip of the blade. Looking at the effect on the 1T mode in Figure 30 the difference is very similar to that of the 1R mode in appearance with the difference being the magnitude of the |CRES| value.

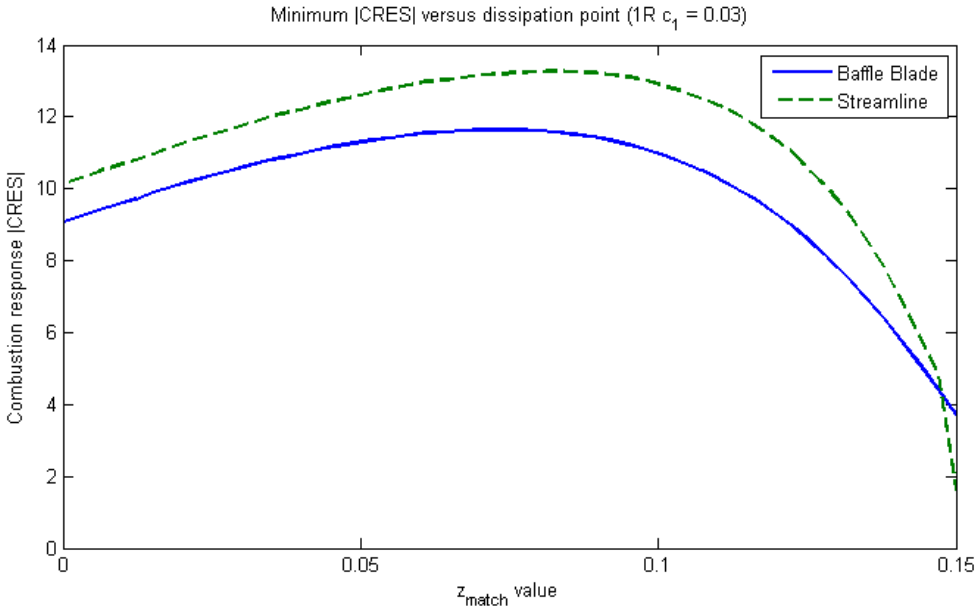

Figure 29: Change in minimum |CRES| with different h_{match} and b_{match} locations for the 1R mode

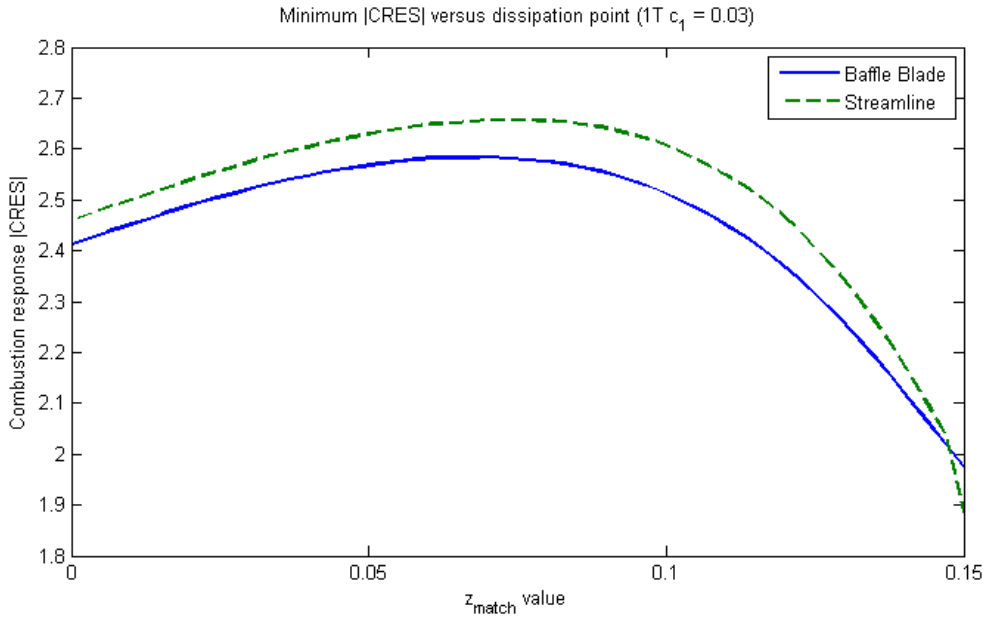

Figure 30: Change in minimum |CRES| with different h_{match} and b_{match} locations for the 1T mode

Due to the small effect that the movement of the matching point had on the predicted dissipation, the decision was made to leave the matching location at the baffle blade. This is a location which is considerably easier to define and requires no extra calculation.

4.5: Geometry Effects

Figures 31 and 32 indicate how the energy dissipation rate changes as the baffle length and the baffle thickness is changed for a 1T acoustic-oscillation mode with a c_1 value of 0.03. It should be noted that the variable, v_{diss}, plotted on the y axis is the total energy dissipation for the baffle blades. Similar results were obtained for 1R and 2T oscillation modes. Since a baffle-length scale is now included in the turbulent viscosity formulation, the corner-flow model, as indicated in Figure 31, has a greater dependence on the baffle length than the Baer-Mitchell model, in which the energy dissipation rate is almost independent of baffle length. Of particular importance is the tendency of the corner flow model to approach zero as the baffle length nears zero. This effect is not mirrored in the Baer-Mitchell model and has been of particular concern. The corner flow model also appears to minimize the irregularities present in the Baer-Mitchell model. In Figure 32, the predictions for both models indicate that there is large energy dissipation in the limit of an infinitely thin blade, where the tip velocities would be infinite. There is also a local minimum at a relatively large baffle thickness. The computations were performed up to where the baffle thickness is equal to the baseline baffle length of 0.1 which would result in a nearly square baffle blade.

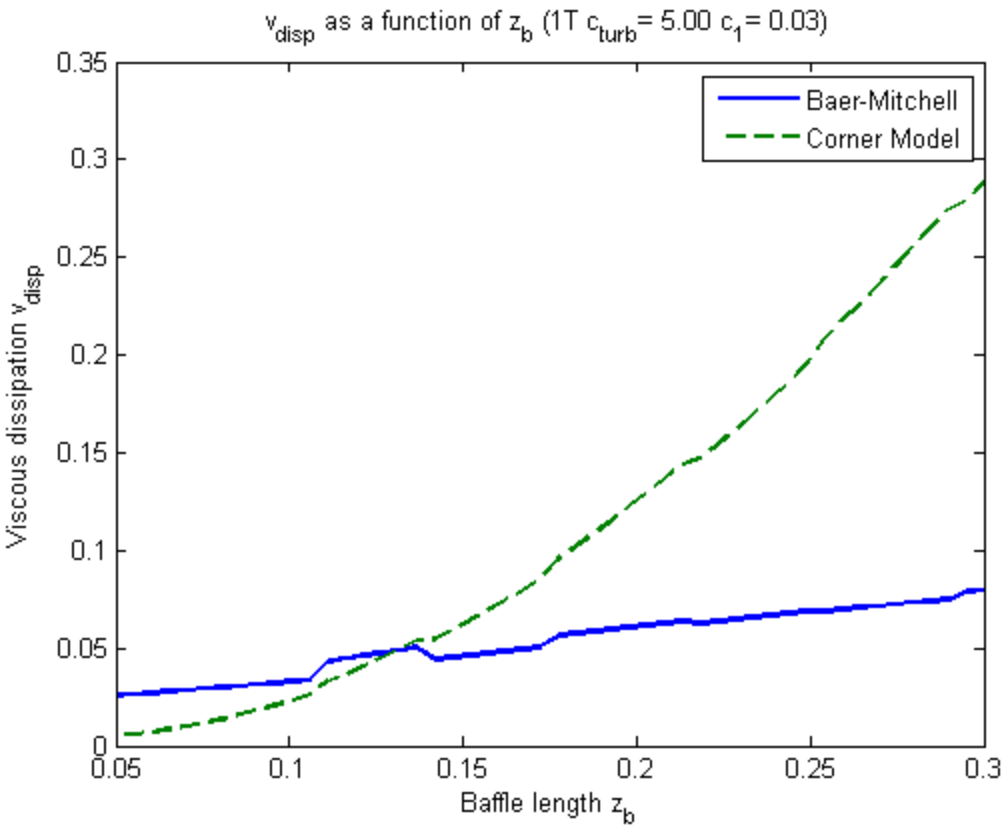

Figure 31: Energy dissipation rate as a function of baffle length for 1T mode t = 0.05

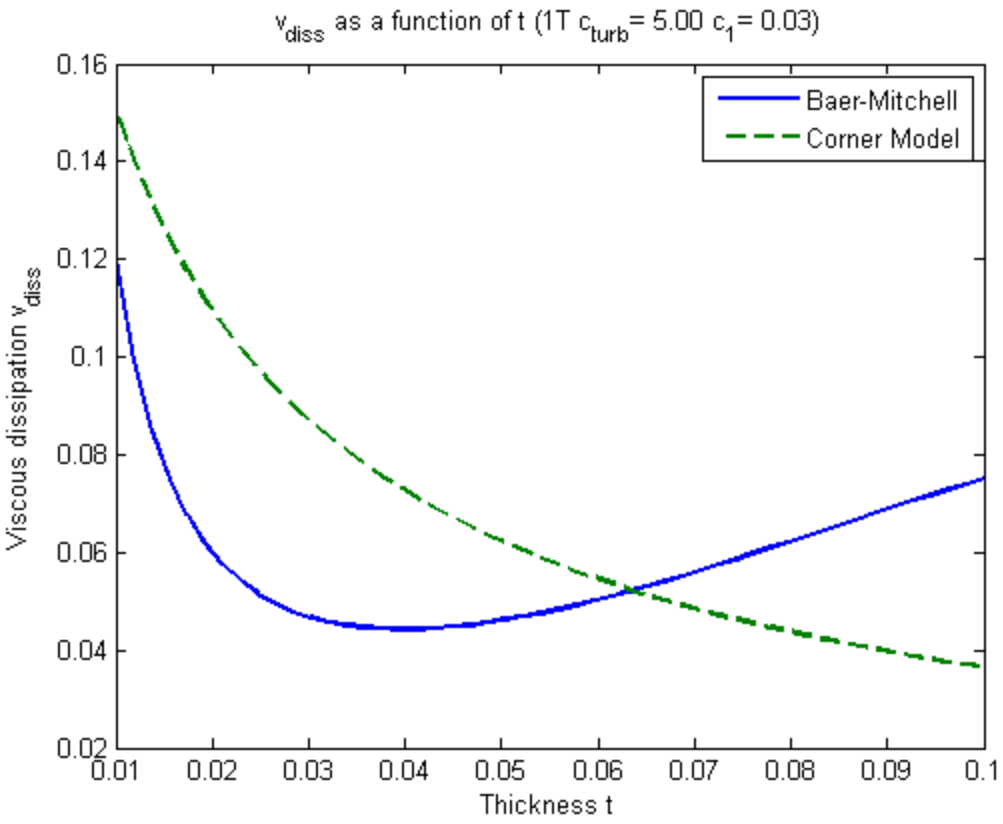

Figure 32: Energy dissipation rate as a function of baffle thickness for 1T mode z_b = 0.15

The Baer-Mitchell model also seems to predict the minimum due to baffle thickness to occur somewhere around 0.04 while the corner-flow model's minimum is at a larger thickness. The variation in ν_{diss} between the two models for the baffle thickness is relatively small when compared to the variation due to baffle length however.

4.6: Stability Plots

As a final demonstration of the corner-flow model several different n-τ and |CRES|-ω stability plots are included. The baseline overall hub/blade geometry had 5 blades, with a hub radius of r_h = 0.4, blade thickness t = 0.05 and blade length z_b = 0.15. First are plots demonstrating the variation in stability for the 1T mode as the number of baffle blades is increased. The minimum value is that of a clean chamber and the plots above it are for numbers

of baffles ranging from 2 to 7. A c_1 value of 0.03 was used. As can be seen in Figure 33, an increase in the number of baffles for the 1T mode implies a increase in the amount of dissipation with Figure 34 demonstrating the same behavior but |CRES| values. Note that there is a decreasing stability improvement as the number of blades are increased.

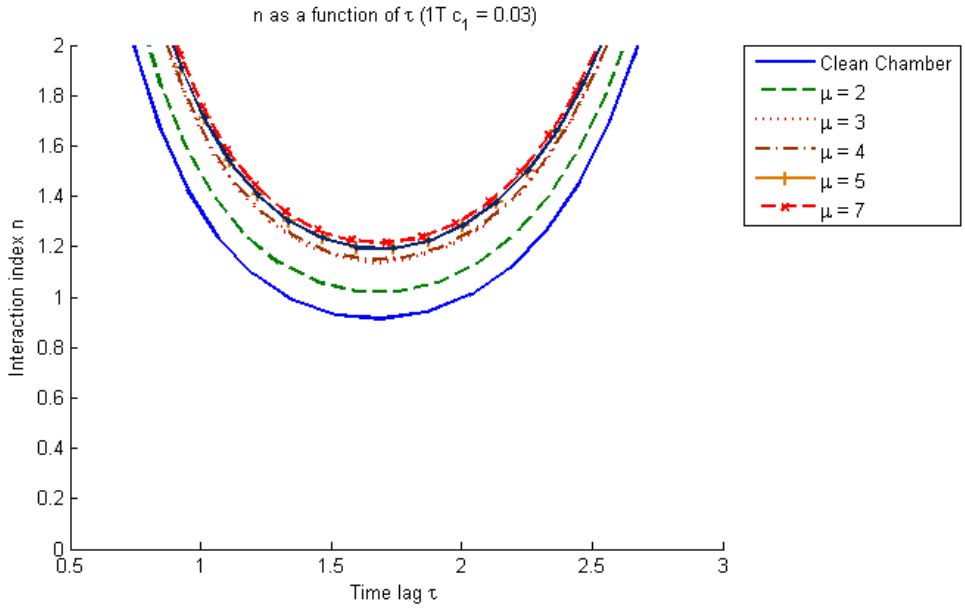

Figure 33: n-τ curves for different baffle arrangements for the 1T mode

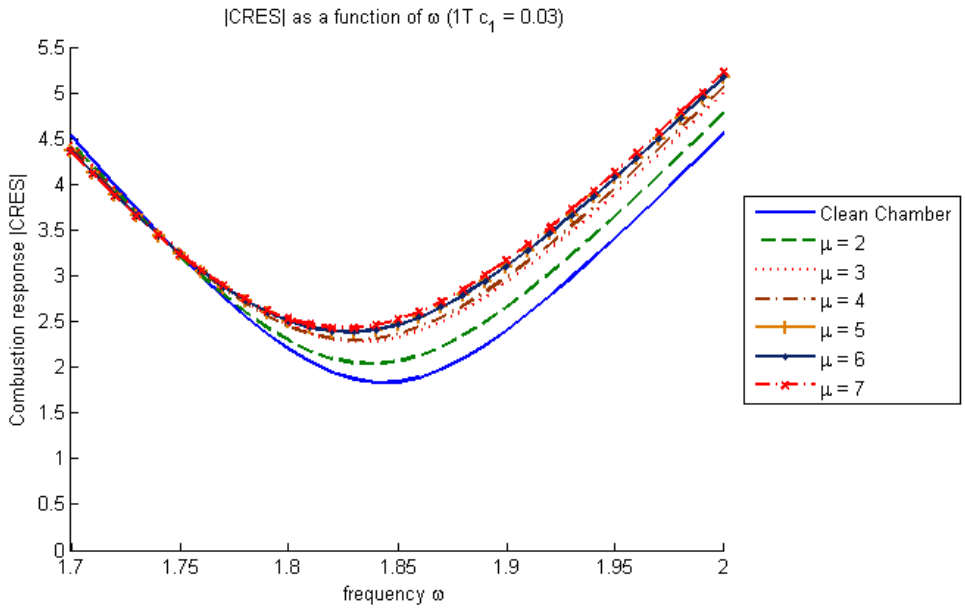

Figure 34: |CRES| curves for different baffle arrangements for the 1T mode

Figure 35 however demonstrates the phenomena that if a baffle blade structure of 2^n is used for a 2T mode the radial baffles are located at velocity nodes so the dissipation only occurs on the hub structure. It is presented here to demonstrate the code works correctly when such a situation is presented. To illustrate this phenomena, the dissipation at each quadrature point has been plotted in in Figure 36. Due to this, designers must choose blade arrangements which do not ignore oscillatory modes commonly observed in a combustion chamber. 2T modes are relatively common, and as such blade arrangements of 2 and 4 baffles are inadvisable.

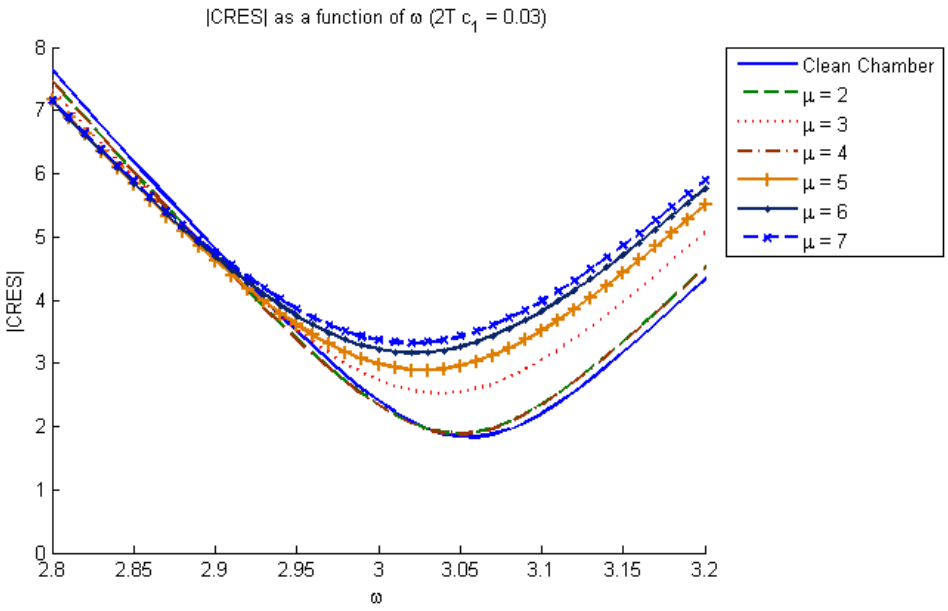

Figure 35: |CRES| for different baffle arrangements for the 2T mode

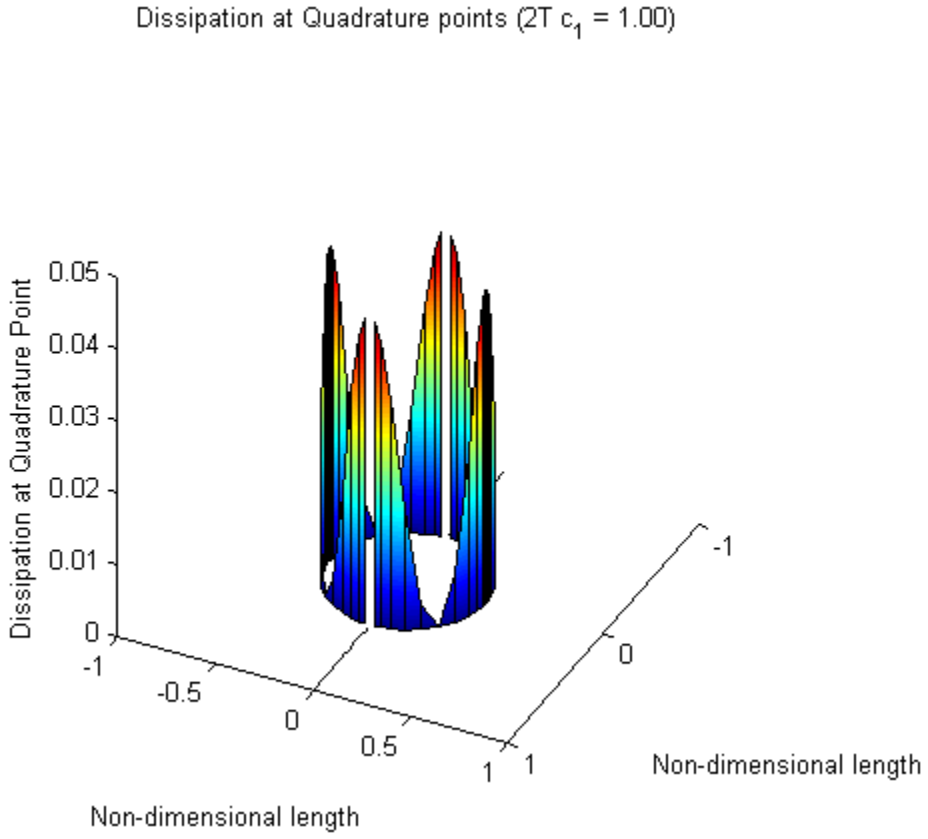

Figure 36: Dissipation at quadrature points for a 2 bladed baffle structure. 2T mode

Variation of the radius of the hub on the stability curves was also performed. Hub radius values were changed from 0.1 to 0.8. It should be noted that in the stability code being used, hub sizes less than 0.1 are not allowed by the stability code.

There appears to be a design point at which the optimal dissipation is reached seen in Figure 37 and 38. After the hub has passed a value between 0.5 and 0.6, the stability curves begin to show the engine is becoming more unstable. This is likely due to the potential difference between the region outside of the hub and the region inside of the hub's potential values becoming smaller. This is observed in many combustion chambers in application. Placement of the baffle at the location of largest potential gradient ensures that the baffle is at its most effective location assuming that the wave form does not change significantly.

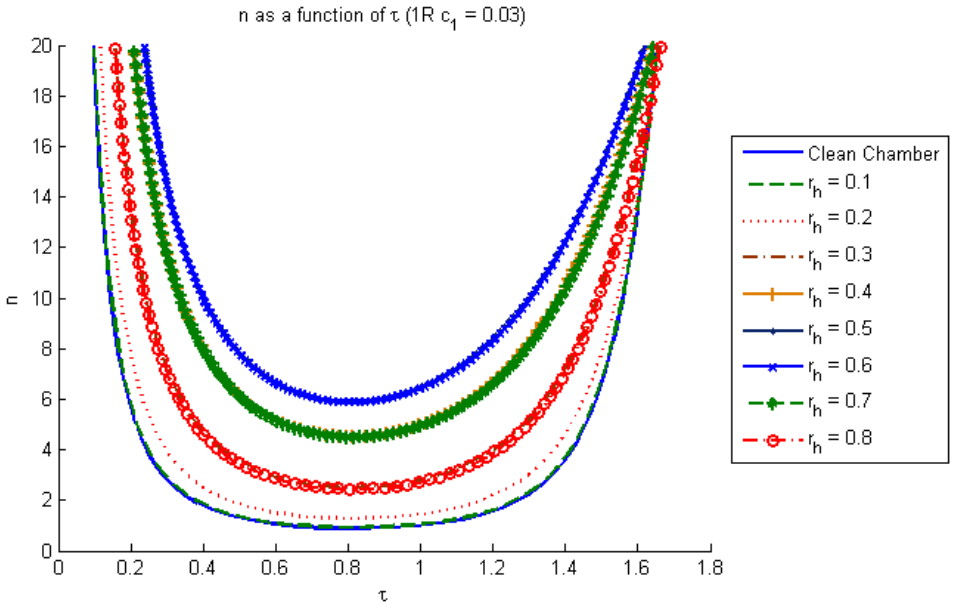

Figure 37: n-τ as a function of hub radius changes (1R, c_1 = 0.03)

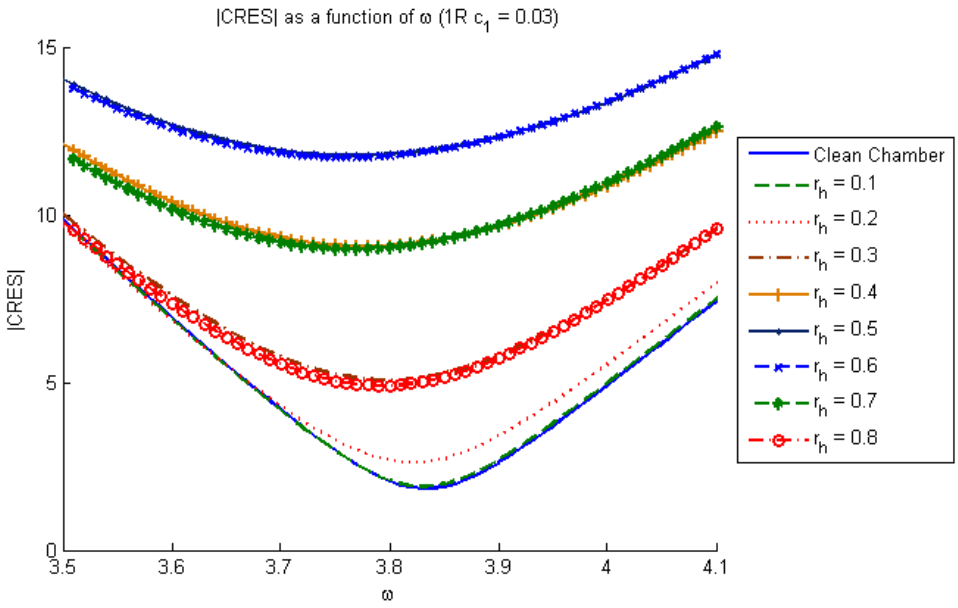

Figure 38: |CRES| as a function of hub radius (1R, c_1 = 0.03)

For the 1T mode it is clear from Figure 39 that a smaller hub is the most efficient method for dissipating wave energy. This is due to the increase in surface area of the radial baffles at smaller hub sizes. The hub plays a much smaller role in the dissipation of a tangential wave's energy. Figure 40 demonstrates the 1T mode stability plotted with |CRES|. This shows essentially the same results but plotted using the different variable representation.

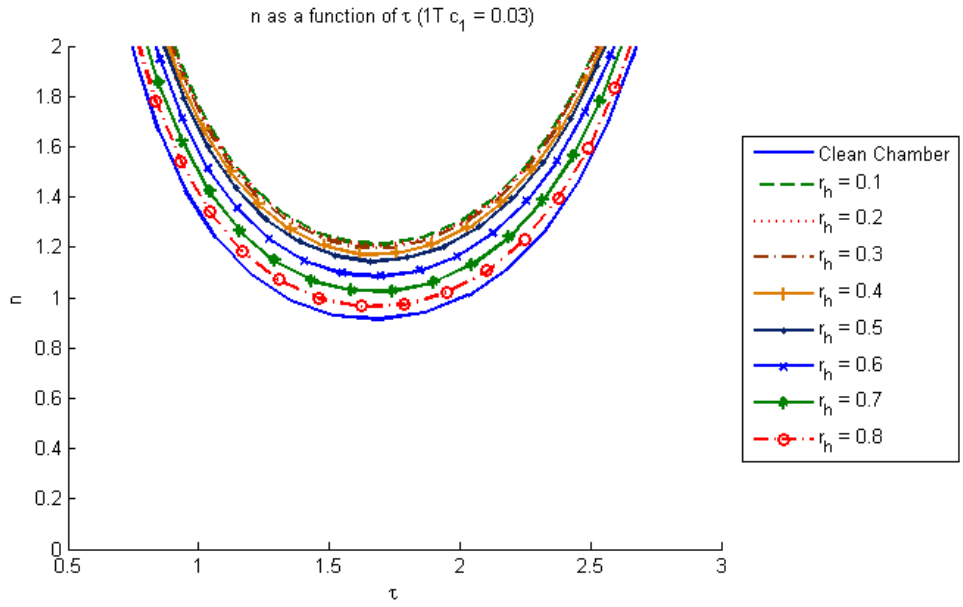

Figure 39: n τ curves as a function of central hub radius (1T, $c_1 = 0.03$)

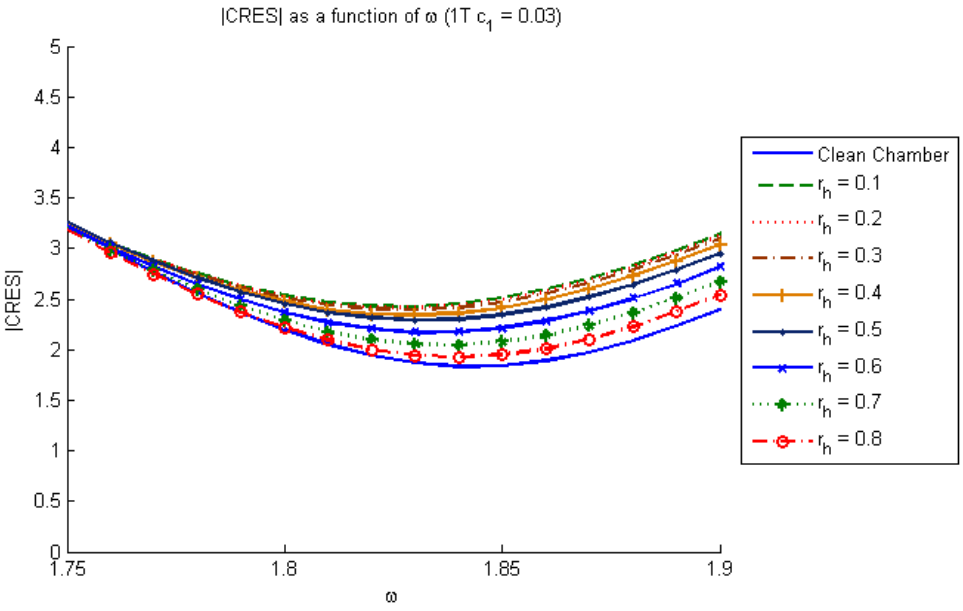

Figure 40: |CRES| curves as a function of central hub radius (1T, $c_1 = 0.03$)

Viewing the resultant stability curves while varying the length of the baffles also yields some useful information. As seen in Figure 41, the engine responds positively in terms of increasing stability for longer baffle blades. This is as expected given the results in Figure 41 and are mirrored in the |CRES| curves of Figure 42. Of note is the increase in natural frequency of the minimum |CRES| combustion chamber as the length of the baffles is increased.

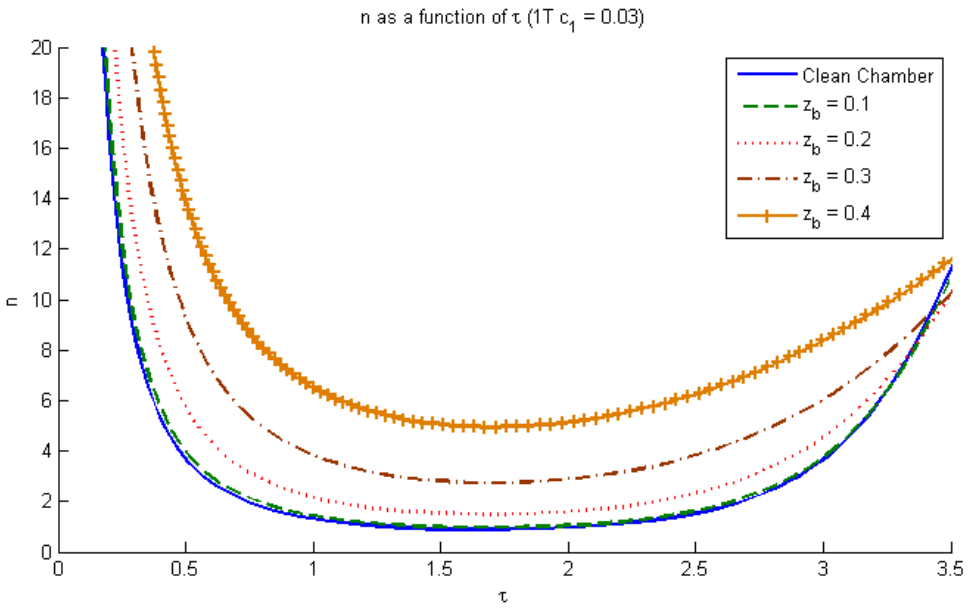

Figure 41: Effect of varying baffle length for 1T mode

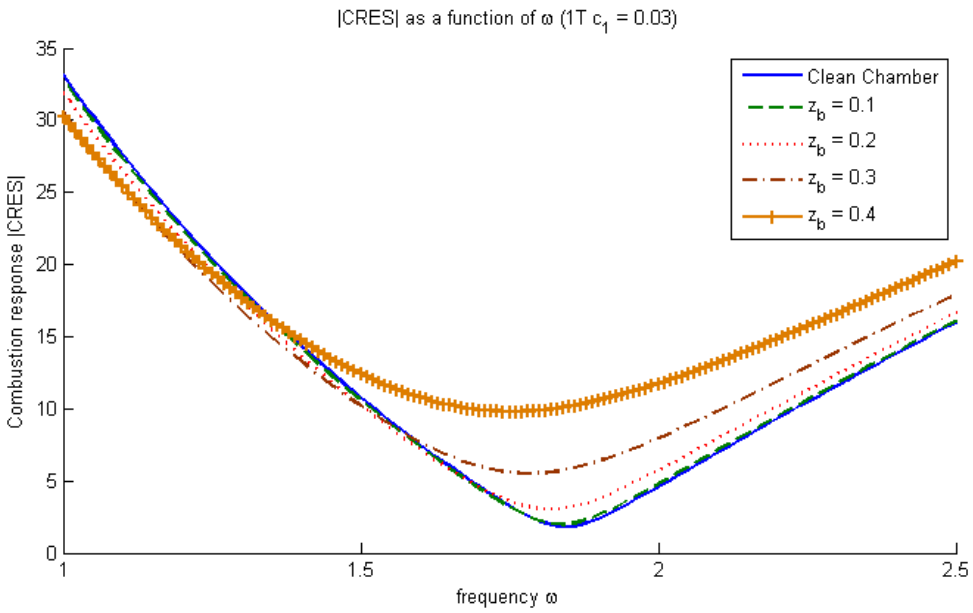

Figure 42: |CRES| as a function of baffle length of 1T mode

5: Summary and Conclusions

The rate of energy dissipation of the baffle blades in a liquid-fueled rocket combustion chamber was computed using a corner-flow viscous flow model that included unsteady flow separation and turbulence effects. For the inviscid portion of the flow field, a velocity potential methodology was formulated using an eigenfunction expansion and a velocity-potential matching technique. Parameters such as local velocity, elemental path length, effective viscosity, and local energy dissipation rate were computed as a function of the local streamline angle α for a representative baffle blade, and compared to results predicted by the Baer-Mitchell blade dissipation model.

The overall baffle energy dissipation rate was also calculated for a hub/blade baffle configuration in a representative test engine. Through the inclusion of a length scale in the turbulent viscosity equation, the corner-flow model shows a much greater dependence on the baffle length than the Baer-Mitchell model. The corner-flow model also predicts no dissipation when the baffle length is zero.

The potential match point was made at the baffle blade to reduce computation time and have the potential difference computed at an easily definable position. A methodology for determining the turbulence coefficient c_1 was developed, and upon comparison with previous results a value of $c_1 = 0.03$ was chosen.

Stability plots showed that the addition of additional baffle's has a diminishing return as far as increased stability. The model also predicts that certain baffle arrangements are, essentially, invisible to various tangential modes. Variation of the size of the hub was also performed and the effects of a larger hub size on the stability curves were observed. The design point for maximum dissipation of the 1R mode at approximately half of the chamber's radius was

accurately predicted. The reduction in stability for the 1T mode as the radial blade's surface area was reduced with increasing hub radius was also observed. Increasing the baffle length was shown to have an increase in the overall stability of the combustion chamber.

References

1. Harrje, D. T., and Reardon, F. H. (eds.), “Liquid Propellant Rocket Combustion Instability,” NASA SP-194, (1972).

2. Mitchell, C. E., “Analytical Models for Combustion Instability”, Liquid Rocket Engine Combustion Instability, edited by V. Yang and W. Anderson, Vol. 169, Ch. 15, pp.403-430, 1995.

3. Baer, M. R. and Mitchell, C. E., “Theoretical Evaluation of Rigid Baffles in Suppression of Combustion Instability,” NASA CR-134896, (1976). See also Baer PhD Thesis (1975) Colorado State University.

4. Milano, D., “Analytical Modeling of High Frequency Combustion Instability in Liquid-Fueled Rocket Engines with Baffled Combustion Chambers”, MS Thesis Colorado State University (2008).

5. Milano, D., Kirkpatrick, A. T., Quinlan, J. M., Mitchell, C. E., and Hinerman, T. D., “Computation of Acoustic Oscillations and Combustion Stability in a Rocket Engine with Combined Hub/Blade Baffles”, AIAA-2009-4866, (2009).

6. Oberg, C. L., Evers, W. H., and Wong, T. L., “Analysis of the Wave Motion in Baffled Combustion Chambers”, NASA CR-72897, (1971).

7. Quinlan, J. M., Milano, D., Kirkpatrick, A. T., Mitchell, C. E., and Hinerman, T. D., “Analytical and Numerical Development of a Baffled Liquid Rocket Combustion Stability Code”, AIAA-2009-4865, (2009).

8. White. F. M., “Fluid Mechanics” , McGraw-Hill, (1998).

9. Acker, T., Mitchell, C. E., and Cody, J., “Acoustic Oscillations in a Cylindrical Chamber with a Hub Baffle”, AIAA-99-1977, (1999).

10. Baranek, L., Acoustics, McGraw-Hill, (1954) NY.

11. Fay, J., Introduction to Fluid Mechanics, (1994), MIT Press, Cambridge.

12. Morse, P., and K. Ingard, Theoretical Acoustics, (1968) Princeton Univ. Press. Princeton.

13. Schwarg, A., and J. Janika (eds.), Combustion Noise, (2009), Springer-Verlag, Berlin.

14. Howe, M., Acoustics of Fluid-Structure Interactions, (1998), Cambridge Univ. Press, Cambridge.

15. Wilcox, D., Turbulence Modeling for CFD, (1994), DCW Industries, La Cañada, CA.

16. Raichel, D., The Science and Applications of Acoustics, (2000), Springer-Verlag, NY.

Appendices

Appendix 1: Polar Vibration Solution

The amplitudes of unforced oscillatory systems are found by solving the Helmholtz equation

$$\nabla^2 \cdot A + k^2 \cdot A = 0$$

In this equation ∇^2 is the Laplacian, A is the amplitude, and k is the wave number.

The differential equation of a wave in polar coordinates is:

$$\frac{1}{r} \cdot \frac{d}{dr}\left(r \cdot \frac{d}{dr} A \right) + \frac{1}{r^2} \cdot \frac{d^2}{d\,\theta^2} A + k^2 \cdot A = 0$$

Attempting separation of variables:

$$A(r,\theta) = R(r) \cdot \Theta(\theta)$$

$$\frac{1}{r} \cdot \frac{d}{dr}\left(r \cdot \frac{dR}{dr} \cdot \Theta \right) + \frac{1}{r^2} \cdot \frac{d^2\Theta}{d\,\theta^2} \cdot R + k^2 \cdot R \cdot \Theta = 0$$

$$\frac{r^2}{R} \cdot \frac{d^2 R}{dr} + \frac{r}{R} \cdot \frac{dR}{dr} + \frac{d^2\Theta}{d\,\theta^2} \cdot R + k^2 \cdot r^2 = 0$$

Which can be separated:

$$\frac{d^2\Theta}{d\theta^2}\cdot\frac{1}{\Theta}=-n^2$$

$$\frac{r^2}{R}\cdot\frac{d^2R}{dr^2}+\frac{r}{R}\cdot\frac{dR}{dr}+k^2\cdot r^2=n^2$$

Simplifying the equations:

$$\frac{d^2\Theta}{d\theta^2}+n^2\cdot\Theta=0$$

$$r^2\cdot\frac{d^2R}{dr^2}+2\cdot r\cdot\frac{dR}{dr}+\left(k^2\cdot r^2-n^2\right)\cdot R=0$$

Assuming that the period of Θ is 2π and knowing that with the first derivative term of the Θ equation equaling zero:

$$\Theta=c_1\cdot e^{\alpha\cdot\theta}\cdot\cos(\beta\cdot\theta)+c_2\cdot e^{\alpha\cdot\theta}\cdot\sin(\beta\cdot\theta)$$

Where:

$$\alpha=\frac{-b}{2\cdot a}\quad\beta=\frac{\sqrt{4\cdot a\cdot c-b^2}}{2\cdot a}\quad a=1\quad b=0\quad c=n^2\quad\alpha=0\quad\beta=n$$

The solution in the Θ direction becomes

$$\Theta = c_1 \cdot \cos(n \cdot \theta) + c_2 \cdot \sin(n \cdot \theta)$$

Because for the R section the simplified form is Bessel's equation:

$$R(r) = C_a \cdot J_n(k \cdot r) + C_b \cdot Y_n(k \cdot r)$$

Because Bessel functions of the second kind (Y_n) go to negative infinity at 0 C_b must be equal to zero when there is no hub. For a system where there are spars (drum-head) or baffles (combustion chamber) the boundary condition is defined as:

$$A(r, \theta) \rightarrow A\left(r_o, \frac{2 \cdot \pi}{\mu}\right) = 0 \qquad \frac{dA}{dr}\left(r_o, \frac{2 \cdot \pi}{\mu}\right) = 0$$

For the drum and combustion chamber cases respectively. If there were no baffles the equations would have values of zero for θ.

A hub is included by dividing the equation for R by C_b which effectively non-dimensionalizes the R equation. This makes it so only one matching point is necessary which can be chosen to be the hub. The boundary conditions for a hub for a drum-head and a combustion chamber are given by:

$$A(r_h, \theta) = 0 \qquad \frac{dA}{dr}(r_h, \theta) = 0$$

Additional vibration information is given in references 10-16

Appendix 2: Expanded Non-dimensionalization

The following table demonstrates the method by which variables involved in the calculation of the potential and the energy dissipation are non-dimensionalized.

Dimensional Variable	Symbol	Scaling Parameter	Dimensionless Variable
Pressure	P* (Pa)	$\bar{P}*$	P
Temperature	T* (K)	$\bar{T}*$	T
Density	ρ* (kg/m^3)	$\bar{\rho}*$	ρ
Speed of Sound	a* (m/s)	$\bar{a}*$	a
Radius	r* (m)	Chamber radius: r_c*	r
Length	z* (m)	r_c*	z
Time	t* (s)	$\bar{a}*\cdot r_c*$	T
Frequency	f* (Hz)	$\frac{\bar{a}*}{2\cdot\pi\cdot r_c*}$	ω
Kinematic Viscosity	v* (m^2/s)	$\bar{a}*\cdot r_c*$	v
Oscillatory Particle Velocity	u* (m/s)	$\bar{a}*$	u
Mean Flow Velocity	U* (m/s)	$\bar{a}*$	U
Potential	φ* (m^2/s)	$\bar{a}*\cdot r_c*$	
Energy Dissipation	$E_{diss}*$	Product of Dimensionless Variables	E_{diss}

Appendix 3: Milano Combustion Chamber Representation

The following equations describe the potential values (φ) within the engine chambers. The equations, and their notation, come from Milano[8] and are presented here as a reference.

Main Chamber:
$$\phi^{C}=\sum_{m=0}^{m_C}\sum_{l=1}^{l_C} A^{C}_{m,l}\cdot\cos\left(m\cdot\theta\right)\cdot J_{m}\left(\lambda^{C}_{m,l}\cdot r\right)\cdot Z^{C}_{m,l}\left(z\right)$$

Baffle Compartment:
$$\phi^{\mu}=\sum_{m_b=0}^{m_B}\sum_{l_b=1}^{l_B} A^{\mu}_{m_b,l_b}\cdot\cos\left(\frac{m_b\cdot\mu_B}{2}\cdot\theta\right)\cdot\Psi_{m_b,l_b}\left(r\right)Z^{B}_{m_b,l_b}\left(z\right)$$

Hub Compartment:
$$\phi^{H}=\sum_{m_h=0}^{m_H}\sum_{l_h=1}^{l_H} A^{H}_{m_h,l_h}\cdot\cos\left(m_h\cdot\theta\right)\cdot J_{m_h}\left(\lambda^{H}_{m_h,l_h}\cdot r\right)\cdot Z^{H}_{m_h,l_h}\left(z\right)$$

The function $Z_{m,l}(z)$ for the different compartments is:

Main Chamber:
$$Z^{C}_{m,l}=\frac{e^{i\cdot\sqrt{\tilde{\omega}^2-\lambda^{C\,2}_{m,l}}\cdot(z-L)}+e^{-i\cdot\sqrt{\tilde{\omega}^2-\lambda^{C\,2}_{m,l}}\cdot(z-L)}}{e^{i\cdot\sqrt{\tilde{\omega}^2-\lambda^{C\,2}_{m,l}}\cdot(z_B-L)}+e^{-i\cdot\sqrt{\tilde{\omega}^2-\lambda^{C\,2}_{m_b,l_b}}\cdot(z_B-L)}}$$

Baffle Compartment:
$$Z^{\mu}_{m,l}=\frac{e^{i\cdot\sqrt{\tilde{\omega}^2-\lambda^{B\,2}_{m_b,l_b}}\cdot(z)}+e^{-i\cdot\sqrt{\tilde{\omega}^2-\lambda^{B\,2}_{m_b,l_b}}\cdot(z)}}{e^{i\cdot\sqrt{\tilde{\omega}^2-\lambda^{B\,2}_{m_b,l_b}}\cdot(z_B)}+e^{-i\cdot\sqrt{\tilde{\omega}^2-\lambda^{B\,2}_{m_b,l_b}}\cdot(z_B)}}$$

Hub Compartment:
$$Z^{\mu}_{m,l}=\frac{e^{i\cdot\sqrt{\tilde{\omega}^2-\lambda^{H\,2}_{m_h,l_h}}\cdot(z)}+e^{-i\cdot\sqrt{\tilde{\omega}^2-\lambda^{H\,2}_{m_h,l_h}}\cdot(z)}}{e^{i\cdot\sqrt{\tilde{\omega}^2-\lambda^{H\,2}_{m_h,l_h}}\cdot(z_B)}+e^{-i\cdot\sqrt{\tilde{\omega}^2-\lambda^{H\,2}_{m_h,l_h}}\cdot(z_B)}}$$

Coefficients, $A_{m,l}$, for standing waves:

Baffle Compartment:

$$A^{\mu}_{m',l'}=\frac{\sum_{m=0}^{m_C}\sum_{l=1}^{l_C}A^{C}_{m,l}\cdot\int_{\theta_1}^{\theta_2}\cos(m\cdot\theta)\cdot\left(\frac{m_b'\cdot\mu_B}{2}\cdot\theta\right)\cdot d\theta\cdot\int_{r_H}^{1}J_m\left(\lambda^{C}_{m,l}\cdot r\right)\cdot\Psi_{m_b',l_b'}(r)\cdot r\cdot dr}{\int_{\theta_1}^{\theta_2}\cos\left(m_h\cdot\theta\right)\cdot\left(m_h'\cdot\theta\right)\cdot d\theta\cdot\int_{0}^{r_H}J_{m_h}\left(\lambda^{H}_{m_h,l_h}\cdot r\right)\cdot J_{m_h'}\left(\lambda^{H}_{m_h',l_h'}\cdot r\right)\cdot r\cdot dr}$$

Hub Compartment:

$$A^{H}_{m_h',l_h'}=\frac{\sum_{m=0}^{m_C}\sum_{l=1}^{l_C}A^{C}_{m,l}\cdot\int_{0}^{2\cdot\pi}\cos(m\cdot\theta)\cdot\cos\left(m_h'\cdot\theta\right)\cdot d\theta\cdot\int_{0}^{r_H}J_m\left(\lambda^{C}_{m,l}\cdot r\right)\cdot J_{m_h}\left(\lambda^{H}_{m_h',l_h'}\cdot r\right)\cdot r\cdot dr}{\int_{0}^{2\cdot\pi}\cos\left(m_h\cdot\theta\right)\cdot\cos\left(m_h'\cdot\theta\right)\cdot d\theta\cdot\int_{0}^{r_H}J_{m_h}\left(\lambda^{H}_{m_h,l_h}\cdot r\right)\cdot J_{m_h}\left(\lambda^{H}_{m_h',l_h'}\cdot r\right)\cdot r\cdot dr}$$

Main Chamber:

$$D_1=A^{B}_{m_b,l_b}\cdot\int_{\theta_1}^{\theta_2}\cos\left(\frac{m_b\cdot\mu_b}{2}\cdot\theta\right)\cdot\cos(m'\cdot\theta)\,d\theta$$

$$D_2=\int_{r_H}^{1}\Psi_{m_b,l_b}(r)\cdot J_{m'}\left(\lambda^{C}_{m',l'}\cdot r\right)\cdot r\cdot dr\cdot\frac{\partial Z^{B}_{m_b,l_b}(z_B)}{\partial z}$$

$$D_3=\int_{0}^{2\cdot\pi}\cos(m\cdot\theta)\cdot\cos(m'\cdot\theta)\cdot d\theta\cdot\int_{0}^{1}J_m\left(\lambda^{C}_{m',l'}\cdot r\right)\cdot J_{m'}\left(\lambda^{C}_{m',l'}\cdot r\right)\cdot r\cdot dr\cdot\frac{\partial Z^{B}_{m_b,l_b}(z_B)}{\partial z}$$

$$D_4=A^{H}_{m_b,l_b}\cdot\int_{0}^{2\cdot\pi}\cos(m_h\cdot\theta)\cdot\cos(m'\cdot\theta)\cdot d\theta$$

$$D_5=\int_{0}^{r_H}J_{m_h}(\lambda^{H}_{m_h,l_h}\cdot r)\cdot J_{m'}(\lambda^{C}_{m',l'}\cdot r)\cdot r\cdot dr\cdot\frac{\partial Z^{H}_{m_h,l_h}(z_B)}{\partial z}$$

$$D_6=\int_{0}^{2\cdot\pi}\cos(m\cdot\theta)\cdot\cos(m'\cdot\theta)\cdot d\theta\int_{0}^{1}J_m(\lambda^{C}_{m,l}\cdot r)\cdot J_{m'}(\lambda_{m',l'}\cdot r)\cdot r\cdot dr\cdot\frac{\partial Z^{C}_{m,l}(z_B)}{\partial z}$$

$$A^{C}_{m',l'}=\frac{\sum_{\mu=1}^{\mu_B}\sum_{m_b=0}^{m_B}\sum_{l_b=1}^{l_B}\left(D_1\cdot D_2\right)}{D_3}+\frac{\sum_{m_h=0}^{m_H}\sum_{l_h=1}^{l_H}\left(D_4\cdot D_5\right)}{D_6}$$

The forcing function for the combustion chamber is given by the following equation:

$$F(\phi)=\phi\cdot\left[(1+\gamma)\cdot i\cdot\omega\cdot\frac{d\,\bar{u}}{dz}+(1+\gamma)\cdot\left(\frac{d\,\bar{u}}{dz}\right)^2\right]+\ldots$$
$$\frac{\partial\phi}{\partial z}\cdot\left[2\cdot\bar{u}\cdot i\cdot\omega+\bar{u}\cdot\frac{d\,\bar{u}}{dz}\cdot(5+\gamma)-2\cdot\bar{u}_1\cdot\frac{d\,\bar{u}}{dz}\right]+\ldots$$
$$\frac{\partial^2\phi}{\partial z^2}\cdot\left[\bar{u}^2\right]-\ldots$$
$$N\cdot\left\{\phi\cdot\left[\gamma\cdot i\cdot\omega\cdot\frac{d\,\bar{u}}{dz}+2\cdot\gamma\cdot\left(\frac{d\,\bar{u}}{dz}\right)^2\right]+\frac{\partial\phi}{\partial z}\cdot\left[\gamma\cdot\frac{d\,\bar{u}}{dz}\cdot(2\cdot\bar{u}-\bar{u}_1)\right]\right\}$$

The equation is a combination of the stabilizing effects of the flow and the instability caused by the combustion response N. The first three lines of the above equation are the stabilizing effects of the flow while the final line is the destabilizing effect of combustion on the pressure oscillations